

Published in final edited form as:

Nat Struct Mol Biol. 2022 February; 29(2): 152-161. doi:10.1038/s41594-022-00720-y.

# Structural basis for the context-specific action of the classic peptidyl transferase inhibitor chloramphenicol

Egor A. Syroegin $^{1,*}$ , Laurin Flemmich $^{2,*}$ , Dorota Klepacki $^{3,4}$ , Nora Vazquez-Laslop $^{3,4}$ , Ronald Micura $^{2,\#}$ , Yury S. Polikanov $^{1,3,4,\#}$ 

<sup>1</sup>Department of Biological Sciences, University of Illinois at Chicago, Chicago, IL 60607, USA

<sup>2</sup>Institute of Organic Chemistry, University of Innsbruck, Center of Molecular Biosciences Innsbruck, Innrain 80-82, A-6020, Innsbruck, Austria

<sup>3</sup>Department of Pharmaceutical Sciences, University of Illinois at Chicago, Chicago, IL 60607, USA

<sup>4</sup>Center for Biomolecular Sciences, University of Illinois at Chicago, Chicago, IL 60607, USA

#### **Abstract**

Ribosome-targeting antibiotics serve as powerful antimicrobials and as tools for studying the ribosome, whose catalytic peptidyl transferase center (PTC) is targeted by many drugs. The classic PTC-acting antibiotic chloramphenicol (CHL), as well as the newest clinically significant linezolid (LZD), were considered indiscriminate inhibitors of protein synthesis that cause ribosome stalling at every codon of every gene being translated. However, recent discoveries showed that CHL (and LZD) preferentially arrest translation when ribosome needs to polymerize particular amino acid sequences. The molecular mechanisms that underlie the context-specific action of ribosome inhibitors are unknown. Here, we present high-resolution structures of ribosomal complexes, with or without CHL, carrying specific nascent peptides that support or negate the drug action. Our data suggest that the penultimate residue of the nascent peptide directly modulates antibiotic affinity to the ribosome by either establishing specific interactions with the drug or by obstructing its proper placement in the binding site.

# INTRODUCTION

Protein synthesis is catalyzed by the ribosome, one of the most conserved and sophisticated molecular machines of the cell. Many classes of antibiotics selectively bind the bacterial ribosome and prevent cell growth by interfering with protein synthesis. Ribosome-targeting antibiotics are indispensable both as therapeutic agents and as tools for basic research<sup>1</sup>.

<sup>\*</sup>To whom correspondence should be addressed: ronald.micura@uibk.ac.at (R.M.), yuryp@uic.edu (Y.S.P.). AUTHOR CONTRIBUTIONS

L.F. and R.M. synthesized short tripeptidyl-tRNA mimics; D.K. and N.V.-L. performed the toe-printing analysis; E.A.S. and Y.S.P. designed and performed X-ray crystallography experiments; R.M., N.V.-L., and Y.S.P. supervised the experiments. All authors interpreted the results. E.A.S., R.M., and Y.S.P. wrote the manuscript.

<sup>\*</sup>Authors contributed equally to this work

Understanding the true molecular mechanisms of action of the newest as well as the "classic" ribosome inhibitors is critical not only for our ability to develop new potent antibacterials but also to expand our knowledge about the fundamental principles of ribosome functioning. In most cases, ribosomal antibiotics interfere with protein synthesis by binding at various functional centers of the ribosome and either lock a particular conformation of the ribosome or hinder the binding of its ligands. The catalytic peptidyl transferase center (PTC) located at the heart of the large ribosomal subunit is the site targeted by the broadest array of inhibitors belonging to several distinct chemical classes, including phenicols, lincosamides, oxazolidinones, pleuromutilins, streptogramins, and some macrolides.

One of the oldest and best-studied PTC-targeting antibiotic (and hence "classic") is chloramphenicol (CHL). Although CHL specifically targets bacterial 70S ribosomes, it can also bind to mammalian mitochondrial ribosomes<sup>2–4</sup>, causing major side effects<sup>5,6</sup>. As a result, the clinical usage of CHL is currently limited to low-income countries, where it is used as an affordable alternative to the more expensive antibiotics. Nevertheless, other drugs of this class, such as florfenicol<sup>7</sup>, are widely used in the United States to treat infections in farm animals. However, despite CHL being studied for decades, we still lack a full understanding of the very basic principles underlying either the toxicity or the mode of the drug action for this class.

Multiple structures of CHL bound to vacant ribosomes from different bacterial species located its binding site in the A site of the PTC<sup>8–10</sup>. This observation resulted in the "classic enzymology"-inspired idea that CHL acts as a competitive inhibitor<sup>11</sup> that prevents accommodation of the aminoacyl moiety of any incoming aminoacyl-tRNA (aa-tRNA) into the ribosomal A site, resulting in inhibition of peptide bond formation. However, this commonly accepted model of CHL action fails to explain several of the early experimental observations, such as the differential inhibition of translation of specific templates, including poly-lysine and poly-phenylalanine synthesis, which are inhibited or not by CHL, respectively<sup>12–14</sup>. Additionally, it was shown that the efficiency of the CHL-mediated inhibition of the puromycin reaction strongly depends on the nature of the P-site substrate<sup>14,15</sup>. Altogether, these early findings suggested that CHL-mediated ribosome inhibition may depend on the nature of both A- and P-site substrates<sup>15</sup>.

The initially perceived ability of CHL to indiscriminately inhibit the formation of any peptide bond also conflicts with its role as an inducer of gene expression: activation of CHL resistance genes relies on the antibiotic-promoted arrest of translation at specific codons within upstream regulatory leader open reading frames (ORFs)<sup>16,17</sup>. Thus, to activate the expression of the resistance locus in response to the antibiotic assault, the ribosome should be able to progress through several leader ORF codons to reach the site of the programmed translation arrest. Therefore, it had remained unclear how the ribosome could polymerize a segment of the leader peptide if CHL indiscriminately inhibits the formation of every peptide bond. Detailed analysis of ribosome profiling data of the CHL action in the bacterial cell<sup>18</sup>, as well as *in vitro* primer extension inhibition (toe-printing) assays<sup>18</sup> and single-molecule Förster resonance energy transfer (smFRET)<sup>19</sup> approaches on several representative ORFs, provided clear evidence that CHL does not block the formation of

every peptide bond with the same efficiency but instead interferes with translation in a context-specific manner. The nature of specific C-terminal residues of the nascent peptide, as well as of the A-site acceptor, was found to strongly influence the ability of CHL to inhibit peptidyl transfer. The presence of alanine, and to a lesser extent of serine and threonine, in the penultimate position of the peptide is conducive to CHL-induced ribosome stalling<sup>18,19</sup>. In contrast, glycine in the P or A sites of the PTC strongly counteracts the inhibitory effect of CHL<sup>18,19</sup>. Unfortunately, all of the available structures of bacterial ribosomes associated with CHL show how it binds to the PTC of either vacant ribosomes<sup>8,9</sup> or ribosomes in complex with deacylated tRNA substrates<sup>10</sup>. Therefore, the key missing piece of information that prevents understanding the molecular mechanisms of the context specificity of action of PTC-targeting antibiotics are structures showing how the action of the ribosome-bound drug is affected by the nature of the donor (peptidyl-tRNA) and/or the acceptor (aa-tRNA) substrates. Such structures would closely mimic the state of the ribosome in a living cell at the time of the encounter with the drug and would provide the most accurate information about recognition of the translating ribosome by the antibiotic.

In this work, we report high-resolution structures of *Thermus thermophilus* (*Tth*) 70S ribosomes with or without PTC-targeting antibiotic CHL and containing combinations of peptidyl-tRNA and aa-tRNA analogs that are either conducive to the drug action or render the peptide bond formation reaction immune to the presence of the antibiotic. We found that the CHL binding site is formed not only by the ribosome alone but also by the growing polypeptide chain and, therefore, the shape of the drug-binding pocket is continuously remodeled as the nascent chain is synthesized by the ribosome. Altogether, our results demonstrate that the interplay between the ribosome, the nascent peptide chain, and the ribosome-bound drug defines whether or not ribosome stalling would occur in the presence of the PTC-targeting antibiotics such as CHL.

# **RESULTS**

#### MTI and MAI tripeptides cause CHL-dependent ribosome stalling

The main goal of this study is to gain understanding of the structural bases for the context specificity of CHL action, which may serve as a paradigm for other PTC-targeting drugs acting in a sequence-specific fashion, such as clinically important oxazolidinones. More specifically, we aimed to structurally decipher the role of the amino acid residue at the penultimate (-1) position of the growing polypeptide chain, which was shown to be critical for the action of CHL<sup>18,19</sup>. For our studies, we chose a short tripeptide CHL-stalling motif – Met-Thr-Ile (MTI) – which represents the three N-terminal amino acid residues of the *E. coli osmC* gene<sup>18,20</sup>. Biochemical and *in vivo* experiments suggested that, in the presence of CHL, the ribosome stalls when the third Ile codon is placed in the P site, likely because it fails to form a peptide bond between the donor substrate, peptidyl-tRNA carrying the MTI-tripeptide, and the incoming A-site acceptor substrate, histidyl-tRNA<sup>18,20</sup>. Using a solid-phase chemical synthesis of the short tRNA-substrate analogs mimicking the 3'-terminal CCA-end of the acceptor stem of full-length tRNAs<sup>21</sup>, we generated a peptidyl-tRNA analog carrying the MTI-tripeptide (5'-ACCA-ITM) (Extended Data Fig. 1). In addition, because alanine residues are found more frequently than threonines (or

serines) in the penultimate position of the nascent peptides associated with the sites of the most pronounced CHL action<sup>18</sup>, we also synthesized a peptidyl-tRNA analog carrying the MAI-tripeptide (5'-ACCA-IAM) (Extended Data Fig. 1). Lastly, as a negative control, we prepared an MFI-carrying peptidyl-tRNA analog because ribosome profiling analysis and biochemical experiments have shown that phenylalanine in the penultimate position of nascent chains does not support CHL-dependent ribosome stalling<sup>18,19</sup>. Importantly, the peptide moieties of all three peptidyl-tRNA analogs were attached to the ribose of the A76-equivalent nucleotide via non-hydrolyzable amide bonds (Fig. 1a, c), allowing us to capture the pre-attack state in the structures.

Next, to ensure that the peptides included in the synthesized tRNA analogs indeed support (MTI and MAI) or counteract (MFI) CHL action during translation, we carried out primer extension inhibition assays (toe-printing), which allows detection of the drug-induced ribosome stalling site(s) along mRNAs with single-codon accuracy<sup>20,22</sup>. We used a template containing the first 27 codons of *osmC*, including the first three encoding the WT MTI sequence (*osmC*-MTI), as well as its two mutant versions encoding for the polypeptides starting with the MAI (*osmC*-MAI) or MFI (*osmC*-MFI) sequences. As expected, the addition of CHL to the cell-free translation system programmed with the *osmC* mRNA variants resulted in ribosome stalling at the Ile3 codon of the *osmC* ORF, when the threonine (*osmC*-MTI) or alanine (*osmC*-MAI) residues appeared in the penultimate position of the growing polypeptide chains, respectively (Extended Data Fig. 2, lanes 2 and 4, red arrowhead). In contrast, as expected, the replacement of Thr2 with Phe residue completely abolished CHL-dependent ribosome stalling (Extended Data Fig. 2, lane 6, red arrowhead), which is fully consistent with the reported context specificity of CHL action<sup>18,19</sup>.

#### Peptidyl-tRNA analogs' peptide chains show uniform trajectories

To provide a structural basis for the sequence-specific CHL-mediated ribosome stalling, we first explored whether the nature of the penultimate amino acid residue affects the trajectory of a nascent peptide within the 70S ribosome in the absence of antibiotic. To this end, we prepared a set of complexes containing ACC-puromycin (ACC-PMN) as the A-site substrate (Fig. 1a) and one of the three tripeptidyl-tRNA analogs (Fig. 1c) as the P-site substrate, crystallized them, and determined their structures at 2.4–2.5 Å resolution (Fig. 1b; Table 1). The observed electron density maps for both A- and P-site substrates in all three structures allowed unambiguous modeling of the short aminoacyl- and peptidyl-tRNA analogs in the absence of antibiotic (Fig. 1d-i). Superpositioning of all three structures revealed no substantial differences in the overall conformations of the main peptide chain of the tripeptidyl tRNA analogs (Fig. 2a). Not only do the trajectories of the main chain of the three tripeptides look the same, but even the positions of the main-chain and  $C\beta$  atoms of Thr2, Ala2, or Phe2 are identical (Fig. 2a). Next, because we used short tRNA analogs, it was important to ensure that our structures reflect functionally meaningful states. The alignment of our structures containing peptidyl-tRNA analogs with the previously published structures of the 70S ribosome in the pre-attack state containing either non-hydrolyzable amide-linked (Fig. 2b)<sup>23,24</sup> or native ester-linked full-length aa-tRNAs in the A- and P-sites (Fig. 2c)<sup>25</sup> shows no structural differences in the position of the CCA moieties (Extended Data Fig. 3a-c) or the key 23S rRNA nucleotides around the PTC (Extended Data Fig.

3d-f), suggesting that, in structural terms, the short tripeptidyl-tRNA analogs fully mimic the functionally-relevant pre-attack state of the peptidyl-tRNA. In particular, the orientation of the attacking α-amino group of the aa-tRNA or its analog (ACC-PMN) relative to the carbonyl carbon of the P-site substrate is indistinguishable between the structures harboring full-length tRNAs versus those with short tRNA analogs (Fig. 2b, c; Extended Data Fig. 3ac). Moreover, the overall paths of the tripeptides of the peptidyl-tRNA analogs are similar to those of several other peptides in the nascent peptide exit tunnel (NPET), whose somewhat lower resolution structures were obtained previously using cryo-EM (Extended Data Fig. 4)<sup>26,27</sup>. Importantly, unlike all previous structures of ribosome nascent chain complexes (RNCCs) harboring in cis synthesized peptidyl-tRNAs (for example<sup>26,27</sup>), the peptides in our complexes were not made by the ribosomes that were crystallized after being stalled by CHL and, instead, were introduced in trans. Although it has been previously demonstrated that peptidyl-tRNAs can be introduced in trans and sustain protein synthesis<sup>28</sup>, here we provide evidence that the structures of the peptide backbones of the *in-cis*-synthesized and in-trans-introduced peptidyl-tRNAs are nearly identical and, therefore, represent a functional pre-attack state of the PTC (Extended Data Figs. 3, 4).

Interestingly, the presence of any of the three tripeptides (MTI, MAI, or MFI) in the PTC causes the same re-orientation of the nucleotide A2062 of the 23S rRNA, which rotates by  $\sim 160^{\circ}$  relative to its position in the vacant ribosome into a position where it forms a symmetric trans A-A Hoogsteen base pair with the residue A2503 (Fig. 1g–i). In our structures, the main-chain amide group of the penultimate residues of the MTI-, MAI-, and MFI-tripeptidyl moiety of the P-site substrate forms an H-bond with the N1 atom of the A2062 residue, thereby stabilizing it in the rotated state (Fig. 1g–i). Precisely the same rearrangement has been reported before to be caused by the ribosome-bound CHL antibiotic itself or its derivatives  $^{10,29,30}$ . This side-chain-independent and, therefore, likely uniform interaction of the main chain of the nascent peptide with the 23S rRNA determines the observed orientation of the penultimate amino acid side chain towards the A site.

Altogether, comparisons of the structures revealed that the exact placement and the overall trajectories of all three tripeptides in the NPET of the 70S ribosome are strikingly similar (Fig. 2a), irrespective of their ability to stall ribosomes in the presence of CHL (Extended Data Fig. 2). This result suggests that the observed context specificity of the CHL-induced ribosome stalling is neither due to alternative conformations of the nascent peptide chains within the NPET, as suggested previously<sup>19</sup>, nor it is due to differential peptide-induced conformational changes of the key nucleotides in the PTC acquired prior to the encounter with the drug.

#### The peptidyl-tRNA penultimate residue can interact with CHL

The next step was to determine the structures of the same ribosomal complexes harboring short analogs of aminoacyl- and peptidyl-tRNAs, but now in the presence of CHL. However, after multiple attempts using high concentrations of the drug, we failed to detect any meaningful electron density for the ribosome-bound CHL in its canonical binding site<sup>10</sup>, while we observed clear electron density for the ACC-PMN in the A site and the MTI-or MAI-tripeptidyl-tRNA analogs in the P site. The absence of CHL in the complexes is

likely due to the clash between the methyl-tyrosine side chain of the ACC-PMN analog and the nitrobenzyl moiety of the CHL because they occupy exactly the same space in the A-site cleft of the ribosome, making their simultaneous presence on the ribosome impossible (Extended Data Fig. 5a). These data strongly suggest that the affinity of ACC-PMN for the ribosomal A site is high enough to outcompete CHL from its canonical binding site.

In order to avoid direct competition between the aminoacyl moiety of the A-site substrate ACC-PMN and the CHL molecule, we used synthetic 5'-CACCA-3' oligoribonucleotide, which lacks an attached amino acid and, therefore, mimics the 3'-end of a deacylated tRNA in the A site. Importantly, we found that the CACCA tRNA fragment stimulates the binding of the P-site tripeptidyl-tRNA analogs to the ribosome exactly the same way as ACC-PMN. Thus, using CACCA as a short A-site tRNA analog, we determined two structures of the ribosome in complex with CHL and either MTI or MAI stalling tripeptidyl-tRNA analogs at 2.50 Å and 2.40 Å resolution, respectively (Fig. 3; Table 1). In both structures, the CHL molecule is bound to its canonical site in the PTC (Extended Data Fig. 6)<sup>10</sup> so that the nitrobenzyl moiety of the drug intercalates into the A-site cleft (Extended Data Fig. 6c), a hydrophobic pocket formed by the 23S rRNA residues A2451, C2452, and U2506. Not surprisingly, we were unable to obtain a similar structure with the non-stalling MFI-tripeptide, most likely because its bulky phenylalanine side chain competes with CHL for ribosome binding (Extended Data Fig. 5b). From the obtained structures, it became evident that the MTI or MAI stalling peptides stabilize the ribosome-bound drug by directly interacting with it. With the MTI peptide, the hydroxyl group of the side chain of the penultimate threonine residue forms an H-bond with one of the two chlorine atoms of CHL (Figs. 3b, 4a). The side chain of serine, which is also conducive to CHL-dependent stalling when present in the penultimate position of a nascent chain 18, would have the ability to form the same interaction with CHL. Similar to the threonine of MTI, the penultimate alanine of the MAI stalling peptide stabilizes ribosome-bound CHL through an energetically favorable CH- $\pi$  interaction between the side chain methyl group of alanine (serving as an H-donor) and the CHL nitrophenyl ring (serving as an H-acceptor) located 3.6 Å away from each other (Fig. 4). The energy of CH- $\pi$  type of interactions is estimated to be 1.5–2.5 kcal/ mole<sup>31</sup>, which is comparable with the energy of standard H-bonds (0.5–1.8 kcal/mole)<sup>32</sup>, and should substantially increase the affinity of the drug to the ribosome. The observed specific contacts of the CHL molecule with the side chain of the penultimate residue of the MTI or MAI stalling peptides (Fig. 4) likely results in stronger binding of the drug to the ribosome, which presumably decreases its off-rate and makes it harder for the incoming aa-tRNA to displace the ribosome-bound antibiotic. Importantly, our structures reveal why it is the penultimate amino acid residue (position -1) of the peptidyl-tRNA that plays the defining role in CHL-induced ribosome stalling: the side chains of residues in position -2 (methionine) or position 0 (isoleucine in the P site) protrude away from the CHL binding site, while it is only the side chain of residue at position -1 that faces the ribosomal A site and CHL binding pocket (Fig. 4). Therefore, our structural data rationalize previous findings 18 by showing that, regardless of the nature of amino acids at other positions, it is specifically the penultimate residue of the peptidyl-tRNA that either directly interacts or sterically interferes with the CHL in the PTC and, thus, affects its ability to stall ribosomes.

Our structural studies suggest that the affinity of CHL for the ribosome is strongly influenced by the nature of the nascent peptide. We tested this idea by directly measuring the affinity of CHL to ribosomes carrying either the MAI or MFI nascent peptides used in the structural studies. To this end, we used radioactively labeled [14C]-CHL and measured its affinity to the Tth 50S ribosomal subunits complexed with various combinations of the short tRNA analogs (see Online Methods). Consistent with our model, the addition of the MAItripeptidyl-tRNA analog to the ribosomes stimulates CHL binding by 2 fold (Extended Data Fig. 7, bars 3 vs. 1). Even a more prominent 6–7-fold increase in CHL binding was observed when MAI-tripeptidyl-tRNA analog was added to the ribosomes along with the CACCA ligand (Extended Data Fig. 7, bars 5 vs. 1), which, consistent with our structural data, serves as a short analog of deacylated A-site tRNA and substantially increases occupancy by the P-site substrate. In contrast to the effect observed with the MAI-tripeptide, the MFI-tripeptidyl-tRNA analog did not stimulate CHL binding (Extended Data Fig. 7, bars 4 vs. 1), which is also consistent with our model. According to our structural studies, the bulky phenylalanine residue in the (-1) position of the MFI nascent chain is not compatible with the ribosome-bound CHL and, therefore, is expected to decrease CHL binding to such ribosome complex. Our in vitro affinity assays, however, revealed only a moderate inhibition of CHL binding in the presence of MFI-tripeptidyl-tRNA analog (Extended Data Fig. 7, bars 4 and 6 vs. 1). The seeming contradiction with the structural data could be due to the limitations of our affinity assay set-up, where a possible incomplete saturation of the ribosomes with the MFI-tripeptidyl-tRNA would leave a large fraction of vacant ribosomes in the system that are still able to bind the drug. Alternatively, CHL may be able to outcompete the ribosome-bound MFI-tripeptidyl-tRNA when present at high concentrations required for the assay. Importantly, the addition of macrolide antibiotic erythromycin (ERY) to the ribosome complex containing MAI-tripeptidyl-tRNA almost fully eliminates CHL binding (Extended Data Fig. 7, bar 7 vs. 5), which is in excellent agreement with the previous data showing direct competition of CHL and ERY for binding to the ribosome<sup>10</sup>. This control experiment also confirms that the observed binding of [14C]-CHL in our system is specific to the canonical CHL site.

# **DISCUSSION**

Our structural and biochemical data allow us to unambiguously discriminate between the two models – the increased affinity model and the drug-induced conformational rearrangement model – that were proposed to explain the observed context-specificity of CHL action *in vivo* and *in vitro* <sup>18</sup>. Our data firmly support the *increased affinity model*. Apparently, the affinity of CHL for a peptide-free ribosome is not high enough for the drug molecule to efficiently compete with an incoming aminoacyl-tRNA, which is reflected in poor drug-induced ribosome stalling during the first few rounds of elongation on many mRNA templates <sup>18,20</sup>. However, once the emerging peptide reaches a certain length (3–6 amino acids), it becomes better anchored in the NPET and could now provide an additional binding interface for the CHL molecule, especially if the peptide carries alanine, serine, or threonine in the penultimate position, which serve as specific interacting partners for CHL, increasing its affinity for the ribosome and possibly stimulating the rate of drug binding or decreasing the rate of drug dissociation. The CHL molecule, now firmly anchored in

the A site due to its interaction with the penultimate residue of the stalling peptide, would prevent accommodation of the aminoacyl moiety of the aa-tRNA into the A-site cleft, thereby inhibiting peptidyl transfer (Fig. 5a). As revealed by smFRET studies, the ribosome with tightly bound CHL can fully accommodate the body of the incoming aa-tRNA but is unable to place the acceptor amino acid in the conformation required for productive peptide bond formation, resulting in the rejection of tRNA and continued rounds of aminoacyl-tRNA sampling (Fig. 5a)<sup>19</sup>. Based on our structural data, residues with small side chains such as Ala, Ser, or Thr in the penultimate position of the growing peptide are conducive to CHL-dependent ribosome stalling not only because their side chains do not interfere with CHL binding as those of large amino acids might do, but also because their side chains additionally facilitate CHL binding by establishing specific interactions with the drug. In contrast, residues with larger side chains in the penultimate position of the growing peptide are sterically incompatible with CHL and either prevent its binding to the ribosome or cause its dissociation (Fig. 5b). This steric incompatibility of the ribosome-bound CHL and the bulky side chains at the penultimate position of the nascent peptide explains the previously poorly understood inability of CHL to fully inhibit puromycin reaction on polysomes<sup>14</sup>, as well as the inability of CHL to inhibit the puromycin reaction with N-Acetyl-Phe-PhetRNA<sup>Phe</sup> and the poor inhibition of poly(U)-dependent poly-phenylalanine synthesis<sup>15</sup>. Indeed, at any given moment, at least some of the translating ribosomes of the polysome fraction should contain growing peptides with bulky side chains at the penultimate position preventing CHL binding and hence, inhibition. Apparently, during the poly-phenylalanine synthesis, after the first round of transpeptidation and translocation of the dipeptidyl-tRNA into the P site, a phenylalanine residue is always present in the (-1) position of the growing peptide, preventing CHL binding. At the same time, none of these bulky residues interfere with the binding and action of puromycin or an incoming aa-tRNA. Similarly, ribosome profiling studies have shown that adding CHL to bacteria prior to cell lysis still allows the movement of ribosomes by a few codons 18,33,34, potentially reflecting the poor ability of the drug to bind to ribosomes carrying unfavorable nascent chains.

A glycine residue in the penultimate position of the growing peptide should not interfere with CHL binding due to the lack of a side chain (Extended Data Fig. 8a) but, at the same time, would not be able to establish an H-bond or a CH- $\pi$  interaction with the CHL molecule and, hence, is unlikely to increase drug's affinity for the ribosome (Fig. 5c). Nevertheless, with a lesser frequency (compared to that of Ala, Ser, or Thr) glycines do appear at the penultimate position of the CHL-dependent ribosome stalling sites revealed by ribosome profiling<sup>18</sup> as well as by our toe-printing analysis (Extended Data Fig. 2, lanes 2, 4, and 6, green arrowhead), suggesting that absence of interference between the growing peptide and the drug is the primary feature of CHL-stalling motifs. In other words, even if Gly in the penultimate position of the growing peptide chain does not increase the affinity of CHL for the ribosome, at least it does not interfere with CHL binding, a property that contrast with that of all remaining amino acids whose side chains are bulkier than those of Ser or Thr. For example, cysteines and valines have the smallest side chains out of all remaining amino acids and might seem to be comparable in size with Ser or Thr, respectively. However, in silico modeling shows that, due to the 0.4 Å-larger van-der-Waals radius of a sulfur atom compared to oxygen, the Cys residue is actually larger than Ser or

Thr and can barely co-exist with the ribosome-bound CHL molecule (Extended Data Fig. 8b). *In silico* modeling of Val shows that one of its terminal methyl groups clashes with the dichloroacetic moiety of CHL, while the other methyl group comes too close to the CHL nitrophenyl ring (Extended Data Fig. 8c). Altogether, our structural analysis suggests that Cys, Val, or any other residue with a larger side chain in the penultimate position of the growing peptide cannot co-exist with the ribosome-bound CHL and, thus, prevents its binding to the ribosome.

CHL is one of the oldest known PTC-targeting antibiotics and is often viewed as a prototype of this class, whereas oxazolidinone antibiotics are among the newest clinically important ribosome-targeting inhibitors. Even though they are structurally unrelated to CHL, members of the class, such as linezolid (LZD), not only bind and act upon the PTC of the bacterial ribosome <sup>18,19,35</sup> but, remarkably, they exhibit a context-specific mode of action highly similar to that of CHL: they inhibit peptide bond formation one step after an Ala residue appears in the nascent chain <sup>18,19</sup>. In the accompanying paper <sup>36</sup>, using high-resolution cryo-EM structures of oxazolidinone-stalled ribosome complexes, it was demonstrated that the side chain of Ala in the penultimate position of a nascent peptide forms the same  $CH-\pi$  interactions with LZD or radezolid (RZD), another clinicallyimportant oxazolidinone, as it does with CHL in our structures, thereby increasing the affinity of the drugs for the ribosome. Besides CHL and LZD, there are several other classes of ribosome-targeting antibiotics with confirmed context specificity of action<sup>37</sup>, such as NPET-binding macrolides<sup>38</sup>. Although a comprehensive understanding of the macrolide context specificity of action is still lacking, apparently, these translation inhibitors induce ribosome stalling through a mechanism<sup>39-41</sup> that is different from the one described here for CHL.

While the described above rule for context-specific CHL action holds true for the majority of the stalling sites, it is not absolutely strict. The presence of Ala, Ser, or Thr in the (-1) position does not always result in ribosome stalling, and *vice versa*, the stalling may occur even if amino acids other than these are present in the (-1) position, as judged from the toe-printing and ribosome profiling data 18, as well as from the observation that poly-lysine synthesis is sensitive to CHL<sup>15</sup>. Although the orientations of different amino acid residues in the (-1) position of the growing peptide are uniform in all of our structures, the possibility that the nascent chains with different sequences could adopt alternative conformations must be taken into account. Analysis of the multiple structures of RNCCs reported to date reveals variability in the positions of the peptide chains within the NPET, suggesting that the surrounding sequences might affect the orientation of residues in the (-1) position and, thereby, could modulate the strength of CHL binding to the ribosome. For example, the observed ability of Gly in the ultimate (0) position of the nascent chain to effectively overcome CHL-induced ribosome stalling (even when Ala, Ser, or Thr residues are present in the (-1) position)<sup>18</sup> could be explained by destabilization of the (-1) residue conformation due to the increased rotational flexibility of the peptide chain containing a C-terminal Gly. Understanding the effects of more distant residues in the growing peptide on the efficiency of CHL-induced ribosome stalling is not immediately obvious and requires further biochemical and structural investigation.

# **CONCLUSIONS**

The structures reported here rationalize the previous data showing that the presence of Ala, Ser, or Thr in the penultimate position of the nascent peptide is required for efficient CHLinduced ribosome stalling <sup>18,19</sup>. Our results indicate that the CHL binding site is formed not only by the ribosome alone but also by the growing polypeptide, and the shape of the drugbinding pocket continuously changes as the nascent chain is synthesized by the ribosome. In our view, the CHL-induced ribosome stalling occurs because the aminoacyl moiety of an incoming A-site tRNA is unable to displace the tightly bound CHL molecule from its canonical binding site, which happens when it is stabilized by interactions with the proper penultimate residue of the growing peptide, and, therefore, cannot get accommodated into the ribosomal A site making peptide bond formation unattainable 19. From this perspective, the nascent peptide plays the role of drug-affinity modulator <sup>19</sup> and should be considered as a part of the CHL or LZD binding site. Thus, these drugs should no longer be considered as competitive ribosome inhibitors but rather classified as uncompetitive inhibitors – a rare class of enzyme inhibitors, which bind adjacent to the active site of an enzyme and require a substrate to be present prior to their binding (e.g., inhibition of inosine-monophosphate dehydrogenase by mycophenolic acid<sup>42</sup>).

# **ONLINE METHODS**

#### Synthesis of hydrolysis-resistant A-site aminoacyl- and deacyl-tRNA analogs.

Synthetic aminoacyl-tRNA mimic, adenosine-cytidine-cytidine-puromycin (ACC-PMN) was obtained from Horizon Discovery Inc. (Chicago, IL, USA). Synthetic deacyl-tRNA mimic, pentanucleotide 5'-CACCA-3', was obtained from Integrated DNA Technologies (Coralville, IA, USA).

#### Synthesis of hydrolysis-resistant peptidyl-tRNA analogs.

The tripeptidyl-tRNA conjugates featuring MTI, MAI, ot MFI peptide sequences were produced as outlined in Extended Data Fig. 1a and as described below. The DMTO-rA3′-NH-Ile-NHFmoc solid support 1 (Extended Data Fig. 1a) for the synthesis of ACCA-Ile-Ala-Met, ACCA-Ile-Thr-Met, and ACCA-Ile-Phe-Met conjugates was produced according to the following references<sup>43–45</sup>. The assembly of the conjugates was based on Fmoc peptide solid-phase synthesis and RNA solid-phase synthesis using 2′-*O*-[(triisopropylsilyl)oxy]methyl (TOM) protected nucleoside building blocks as outlined in Extended Data Fig. 1a and as described below, essentially based on the reference<sup>21</sup>

1. Solid-phase peptide assembly on the solid support 1. In an ABI synthesis cartridge, solid support 1 (40 mg) was soaked with dry *N*,*N*-dimethylformamide (2 mL, 30 min). For deprotection of the *N*α-Fmoc group, the solid support was treated twice with piperidine solution (20% in *N*,*N*-dimethylformamide, 1.5 mL, 2 min, 15 min) and subsequently washed with *N*,*N*-dimethyl-formamide (3 × 2 mL). Coupling was performed by adding *N*,*N*-diisopropylethylamine (17 μL) to a solution (500 μL) of 100 mM (1-cyano-2-ethoxy-2-oxoethylidenaminooxy)dimethylaminomorpholino-carbenium-hexafluorophosphate and Fmoc-protected amino acid

(100  $\mu$ mol) in *N,N*-dimethylformamide. After 1 minute of preactivation, the solid support was treated with this solution for 1.5 hours. This step was performed twice. Then, the solid support was washed with *N,N*-dimethylformamide (3 × 2 mL), methanol (3 × 2 mL), and dichloromethane (3 × 2 mL) and dried on high vacuum.

- 2. Solid-phase RNA assembly on the tripeptidyl solid support 1. The ACCA moiety was assembled using a Nucleic Acid Synthesizer (ABI 392) following standard synthesis protocols. Detritylation (120 s): dichloroacetic acid/1,2-dichloroethane (4/96); coupling (360 s): phosphoramidites (0.1 M in acetonitrile) were activated with benzylthiotetrazole (0.3 M in acetonitrile); capping (2 × 10 s, Cap A/Cap B = 1/1): Cap A: 0.49 M N,N-dimethylaminopyridine in acetonitrile, Cap B: acetic anhydride, 2,4,6-collidine, acetonitrile (10/15/25); oxidation (20 s): I<sub>2</sub> (0.2 M) in tetrahydrofuran/pyridine/H<sub>2</sub>O (35/10/5). Amidites, benzylthiotetrazole, and capping solutions were dried over activated molecular sieves (4Å) overnight.
- 3. **Deprotection of the 3'-tripeptidyl-ACCA conjugates.** (A) Fmoc and cyanoethyl deprotection. In the ABI synthesis column, the solid support was treated with a solution of 20 % piperidine in acetonitrile (5 mL, 5 min), washed with acetonitrile (3 × 2 mL), and dried. (B) Acyl deprotection and cleavage from the solid support. For the conjugates synthesized on solid support 1, the beads were transferred into a screwcap vial, and equal volumes of aqueous methylamine (33% m/m), and concentrated aqueous ammonia (28–30% m/m) were added. After 20 minutes at 65 °C, the supernatant was filtered and evaporated to dryness. (C) 2'-O-TOM deprotection. The obtained residue was treated with tetrabutylammonium fluoride trihydrate (TBAF·3H<sub>2</sub>O) in tetrahydrofuran (1 M, 1 mL) overnight at room temperature. The reaction was quenched by the addition of triethylammonium acetate (TEAA) (1 M, pH 7.4, 1 mL). After evaporating tetrahydrofuran, the solution was applied on a size-exclusion chromatography column (GE Healthcare, HiPrep 26/10 Desalting, 2.6 × 10 cm, Sephadex G25). By eluting with H<sub>2</sub>O, the conjugate-containing fractions were collected, evaporated to dryness, and the residue was dissolved in H<sub>2</sub>O (1 mL). Analysis of the crude products was performed by anion-exchange chromatography on a Dionex DNAPac PA-100 column (4 × 250 mm) at 80°C. Flow rate: 1 mL min<sup>-1</sup>; eluent A: 25 mM Tris-HCl (pH 8.0) and 20 mM NaClO<sub>4</sub> in 20% aqueous acetonitrile, eluent B: 25 mM Tris-HCl (pH 8.0) and 0.60 M NaClO<sub>4</sub> in 20% aqueous acetonitrile; gradient: 0–35 % B in A within 28 min; UV detection at  $\lambda$ = 260 nm.
- 4. *Purification of the 3'-tripeptidyl-ACCA conjugate*. The crude deprotected conjugates were purified on a semipreparative Dionex DNAPac PA-100 column (9 × 250 mm) at 80 °C with a flow rate of 2 mL min<sup>-1</sup> (for eluents see above). Fractions containing the conjugate were concentrated to near dryness and diluted with 0.1 M (Et<sub>3</sub>NH)<sup>+</sup>HCO<sub>3</sub><sup>-</sup> and loaded on a C18 SepPak Plus cartridge (Waters, Millipore), washed with H<sub>2</sub>O, and eluted with H<sub>2</sub>O/CH<sub>3</sub>CN (1:1). Conjugate-containing fractions were evaporated to dryness and dissolved in H<sub>2</sub>O

(0.5 mL). The quality of the purified conjugate was analyzed by analytical anion-exchange chromatography (for conditions, see above). The molecular weight of the synthesized conjugate was confirmed by LC-ESI mass spectrometry (Extended Data Fig. 1b). Yields were determined by UV photometrical analysis of conjugate solutions.

#### Toe-printing analysis.

For the toe-printing analysis of the CHL-mediated ribosome stalling during *in vitro* translation at the third codon of the *osmC* open reading frame<sup>18</sup>, we used the following DNA template that contains the T7 promoter region, the original first 27 codons (underlined) of the *osmC* gene, followed by a stop codon (\*TAA), and an annealing region for the toe-printing primer NV1:

ATTAATACGACTCACTATAGGGATATAAGGAGGAAAACAT <u>ATG ACA ATC</u>
<u>CAT AAG AAA GGT CAG GCA CAC TGG GAA GGC GAT ATC AAA</u>
<u>CGC GGG AAG GGA ACA GTA TCC ACC GAG AGT GGC</u> \*TAA
GCTCTTTGGTTAATAAGCAAAATTCATTATAACC

This DNA template was prepared by PCR using T7-ermCL-osmC-fwd (5'-ATTAATACGACTCACTATAGGGATATAAGGAGGAAAACATATGACAATCCATAAGA AAGG) and osmC-NV1-reverse (5'-

GGTTATAATGAATTTTGCTTATTAACCAAAGAGCTTAGCCACTCTCGGTGGATACTG TTC) primers. DNA templates containing mutations of the 2<sup>nd</sup> Thr codon (ACA, highlighted in bold in the above sequence) to either alanine (GCA) or phenylalanine (TTC) were prepared by combining forward primer T7-ermCL-osmC-T2A-fwd (5'-

 $\label{eq:attact} ATTAATACGACTCACTATAGGGATATAAGGAGGAAAACATATGGCAATCCATAAGAAAGG) \ or \ T7-ermCL-osmC-T2F-fwd \ (5'-complex or \ T7-ermC-T2F-fwd \ (5'-complex$ 

ATTAATACGACTCACTATAGGGATATAAGGAGGAAAACATATGTTCATCCATAAGAA AGG), respectively, with the same osmC-NV1-reverse primer. Toe-printing analysis was performed essentially as described before  $^{20}$ . Translation time was 5 min and reactions were supplemented with additional 3 mM MgCl $_{2}$ . When added, CHL was at 200  $\mu M$  final concentration.

#### Crystallographic structure determination.

In our initial trials, we tried to either co-crystallize the tripeptidyl-tRNA analogs together with the 70S ribosome or to soak them into the pre-formed ribosome crystals hoping that the analogs would bind into the ribosomal P site leaving the A site vacant. Unfortunately, these initial attempts yielded only poor or no electron density corresponding to the tested synthetic P-site substrates. Increased resolution and significantly better electron density maps resulted from the addition of the aminoacyl-tRNA analog 5'-ACC-puromycin (ACC-PMN) (Fig. 1a), which we have shown previously to be able to strongly bind to the A site of the ribosome and fully mimick aminoacyl-tRNA<sup>23,46</sup>. Further improvement came from the use of the protein Y (PY), which binds to the small ribosomal subunit and is known to improve the resolution of the ribosome complexes<sup>29,30,47,48</sup>. A specific advantage of using the PY in this study results from its ability to compete with the binding of intact tRNAs to the ribosome, which helped to purge any residual ribosome-bound tRNAs that were carried over during

the ribosome purification. In the absence of the competing full-length tRNAs, short peptidyland aminoacyl-tRNA analogs freely bind to the A and P sites on the large ribosomal subunit and can be visualized using X-ray crystallography.

Wild-type 70S ribosomes from *Thermus thermophilus* (strain HB8) were prepared as described previously<sup>48</sup>. Ribosome complexes with *Escherichia coli* PY, and short tRNA analogs were formed by mixing 5 μM 70S ribosomes with 50 μM PY, followed by the addition of 50 μM of one of the three short tripeptidyl-tRNA analogs and 100 μM of either the short aminoacyl-tRNA analog ACC-PMN or the short deacyl-tRNA analog CACCA. All *Tth* 70S ribosome complexes were formed in the buffer containing 5 mM HEPES-KOH (pH 7.6), 50 mM KCl, 10 mM NH<sub>4</sub>Cl, and 10 mM Mg(CH<sub>3</sub>COO)<sub>2</sub>, and then crystallized in the buffer containing 100 mM Tris-HCl (pH 7.6), 2.9% (weight/volume), PEG-20K, 9–10% (v/v) MPD, 175 mM arginine, 0.5 mM β-mercaptoethanol<sup>23,46–48</sup>. Crystals were grown by the vapor diffusion method in sitting drops at 19°C, stabilized and cryo-protected stepwise using a series of buffers with increasing MPD concentrations until reaching the final concentration of 40% (v/v) MPD as described previously<sup>23,46–48</sup>. For 70S ribosome complexes with chloramphenicol, the drug was included in the crystallization mixture (500 μM) and then later added to the stabilization buffers. After stabilization, crystals were flash-frozen using nitrogen cryo-stream at 80°K (Oxford Cryosystems, UK).

Diffraction data were collected using beamlines 24ID-C and 24ID-E at the Advanced Photon Source (Argonne National Laboratory, Argonne, IL) using NE-CAT Remote Access software (version 6.2.0). A complete dataset for each ribosome complex was collected using 0.979Å wavelength at 100K from multiple regions of the same crystal using 0.3-degree oscillations and continuous vector scanning. Processing of the X-ray diffraction data, model building, and structure refinement were essentially performed as described in our previous publications 10,24,30,46–50. Briefly, the raw X-ray crystallographic data were integrated and scaled using XDS software (version from Feb 5, 2021). All structures were refined using PHENIX software (version 1.17). Structural models were built in COOT (version 0.8.2). All figures showing atomic models were generated using PyMol software (version 1.8). The search model was generated from the previously published structures of *T. thermophilus* 70S ribosome in complex with *E. coli* protein Y (PDB entry 4Y4O<sup>48</sup>). The statistics of data collection and refinement are compiled in Table 1.

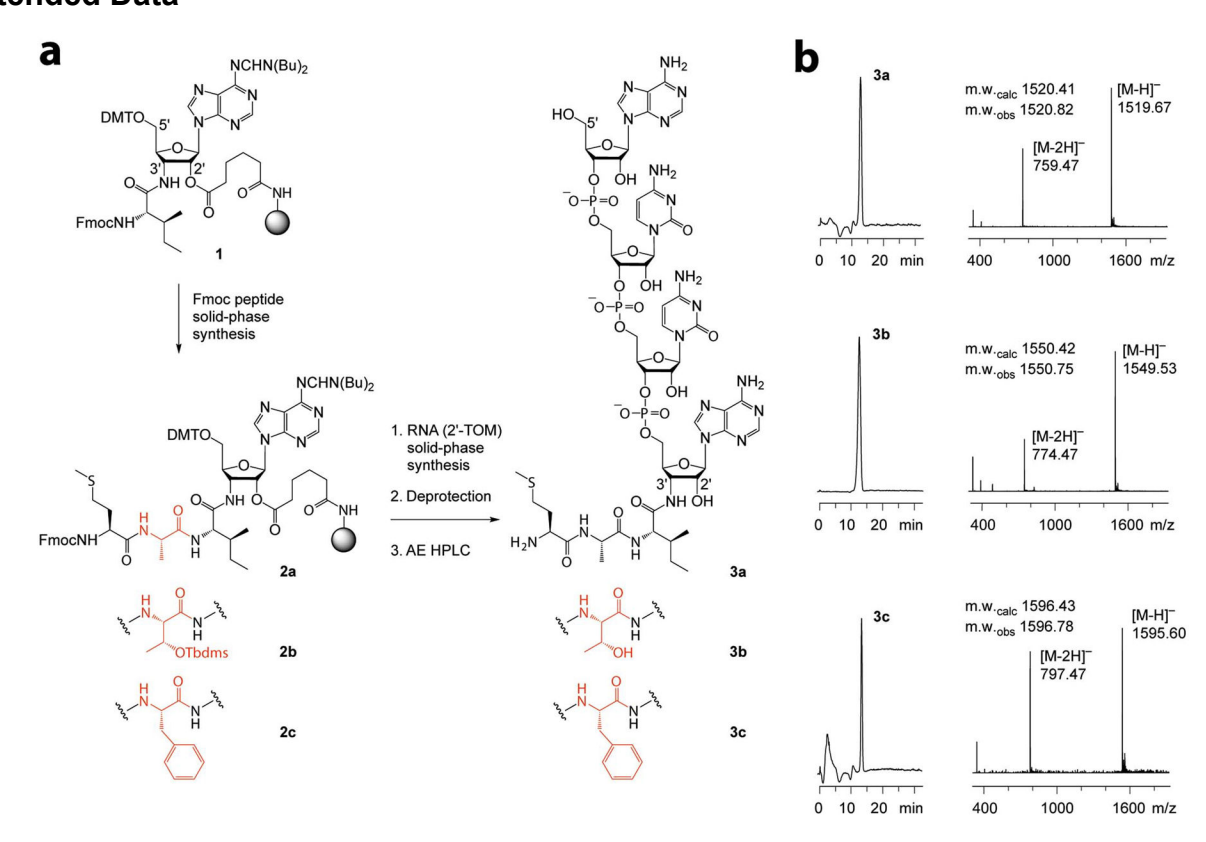
We have also tried to determine similar X-ray crystal structures of oxazolidinone antibiotics (linezolid and tedizolid) with the 70S ribosomes in complex with various A- and P-site substrate combinations, including those that are conducive to linezolid-dependent ribosome stalling. Unfortunately, after multiple attempts, we were unable to observe strong and meaningful electron density for linezolid (as well as tedizolid) bound to the A site of the *T. thermophilus* 70S ribosome. Most likely, these inhibitors have a low affinity for the *T. thermophilus* 70S ribosome. However, comparisons of the available linezolid structures in complex with archaeal (*Haloarcula marismortui*, PDB entry 3CPW<sup>35</sup>) or bacterial (*Deinococcus radiodurans*, PDB entry 3DLL<sup>51</sup>) ribosomes with the structure of the *T. thermophilus* 70S ribosome does not reveal any obvious reasons why linezolid should exhibit poor affinity for *Tth* ribosomes. Importantly, the missing structures of oxazolidinone-

stalled ribosome complexes have been determined using the cryo-EM approach in the accompanying paper<sup>36</sup>.

# In vitro CHL binding assay.

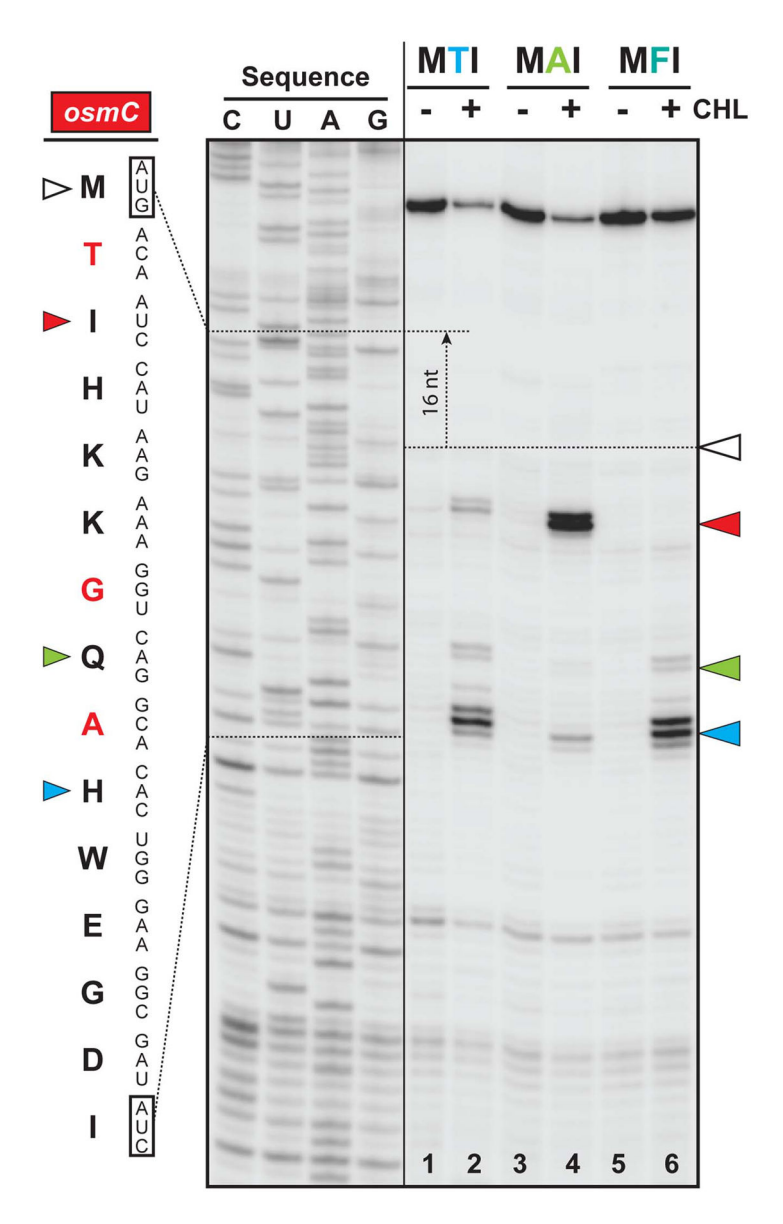
In vitro binding of radioactive CHL to the *Thermus thermophilus* ribosomes in the presence of various combinations of short aminoacyl and peptidyl-tRNA analogs was measured using fragment reaction conditions <sup>52</sup>. Briefly, *Thermus thermophilus* 50S large ribosomal subunits (1.25  $\mu$ M) were incubated in a fragment reaction buffer (50 mM Tris-HCl pH 7.6, 20 mM MgCl<sub>2</sub>, 400 mM KCl) in the presence of various tRNA mimics (50  $\mu$ M CACCA and 25  $\mu$ M ACCA-IAM or ACCA-IFM) and [  $^{14}$ C]-CHL (2  $\mu$ M, 130 dpm/pmole) for 10 minutes at 25°C. Next, 10  $\mu$ L of ethanol were added to 20  $\mu$ L of each reaction mixture, which were then placed on ice for 10 minutes and centrifuged for 10 minutes at 16,000 × g at 4°C to pellet down the ribosomes-CHL complexes. The amount of radioactive [  $^{14}$ C]-CHL remaining in supernatants was measured in a Liquid Scintillation Counter (LS-6000, Beckman-Coulter) by mixing 20  $\mu$ L of supernatants with 5 mL of scintillation liquid (Ultima Gold, Fisher Scientific). 100  $\mu$ M of ERY was used in the control experiment. *Thermus thermophilus* 50S large ribosomal subunits were prepared essentially as 70S used for crystallization by taking the corresponding 50S peak during sucrose gradient ultracentrifugation.

# **Extended Data**



Extended Data Fig. 1. Chemical synthesis of hydrolysis-resistant tripeptidyl-ACCA conjugates.

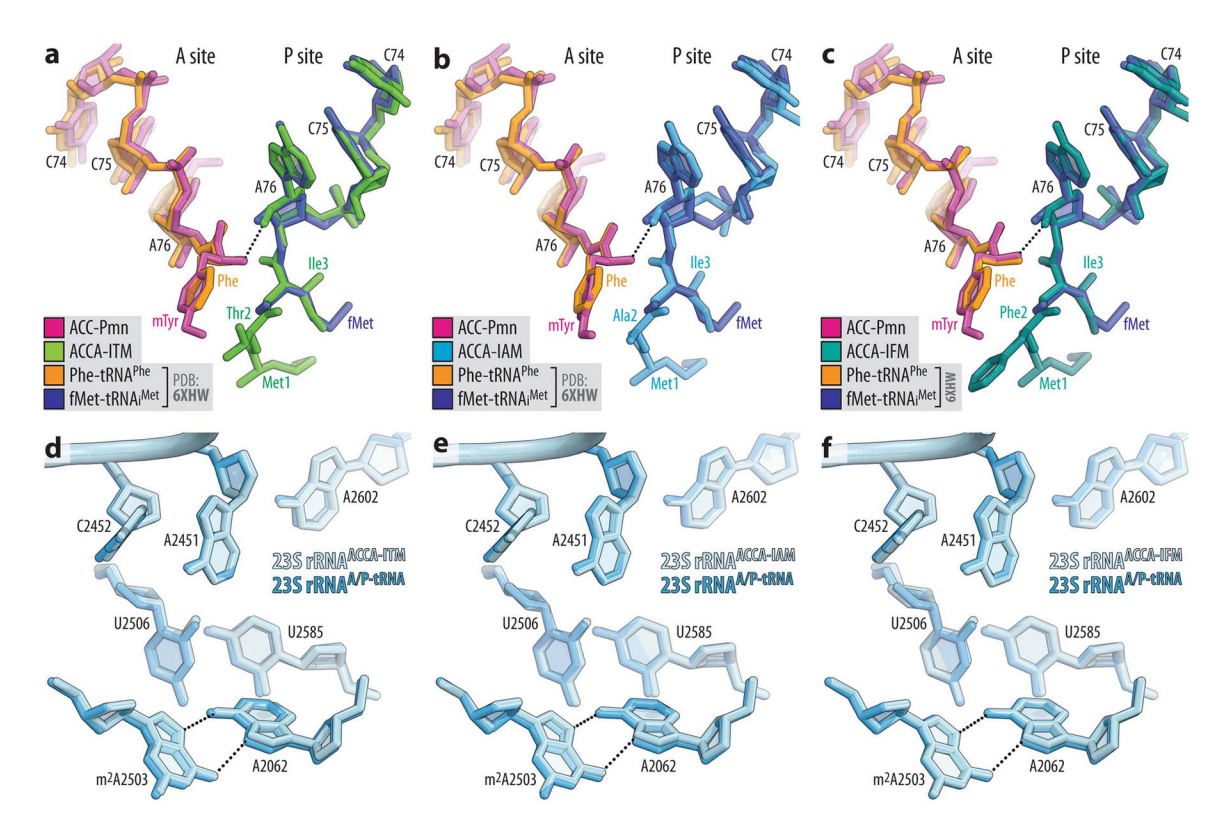
(a) Overview of the synthetic pathway. Chemical structure of functionalized solid support  $1^1$  (grey sphere represents amino-functionalized polystyrene support (GE Healthcare, Custom Primer SupportTM 200 Amino) used for peptide assembly (Fmoc chemistry) and RNA assembly (2'-O-TOM chemistry), followed by deprotection and purification using anion-exchange chromatography; DMT = 4,4'-dimethoxytrityl, Fmoc = N-(9-fluorenyl)methoxy-carbonyl, TOM [(triisopropylsilyl)oxy]methyl, AE HPLC = anion-exchange high-pressure liquid chromatography. (b) Anion-exchange HPLC profiles of purified ACCA-Ile-Ala-Met, ACCA-Ile-Thr-Met, and ACCA-Ile-Phe-Met conjugates (left) and LC-ESI mass spectra (right). Anion-exchange chromatography conditions: Dionex DNAPac PA-100 (4×250 mm) column; temperature: Flow rate: 1 mL/min; eluent A: 25 mM Tris-HCl (pH 8.0) and 20 mM NaClO<sub>4</sub> in 20% aqueous acetonitrile, eluent B: 25 mM Tris-HCl (pH 8.0) and 0.60 M NaClO<sub>4</sub> in 20% aqueous acetonitrile; gradient: 0–35% B in A within 28 min; UV detection at  $\lambda = 260$  nm.



Extended Data Fig. 2. CHL arrests translation at the MTI/MAI tripeptide sequences.

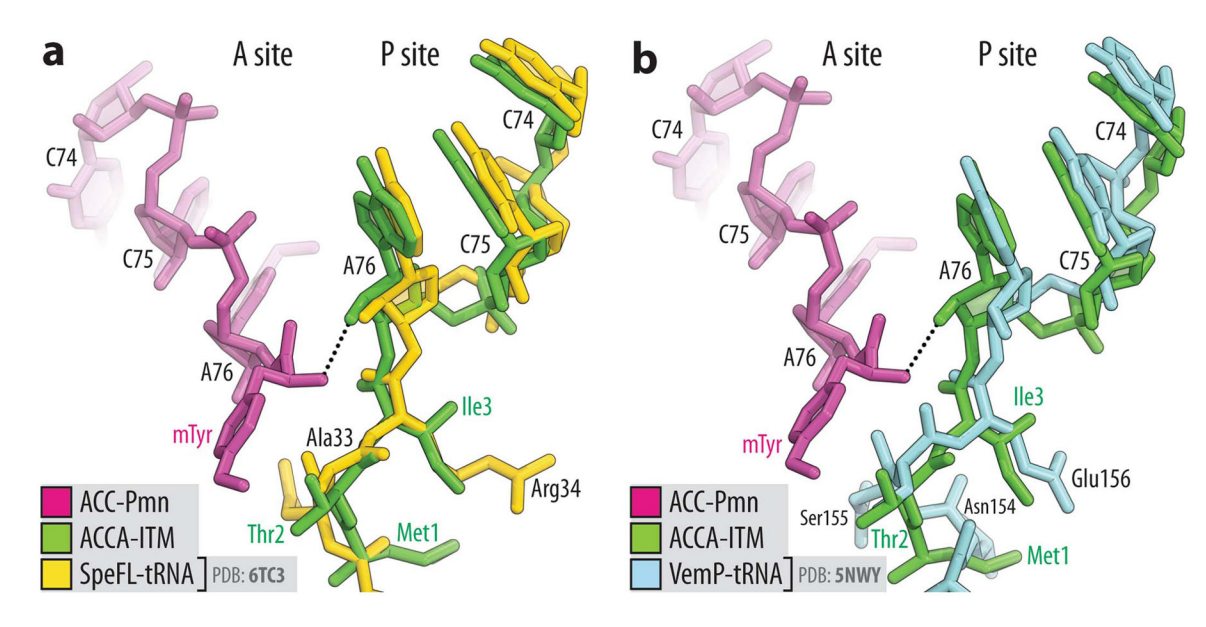
Ribosome stalling in the presence and absence of CHL revealed by reverse-transcription primer-extension inhibition (toe-printing) assay in a cell-free translation system on wild-type osmCmRNA encoding MTI tripeptide at the N-terminus (lanes 1–2) or its mutant versions encoding either alanine (lanes 3–4) or phenylalanine (lanes 5–6) in the 2<sup>nd</sup> position. Nucleotide sequences of wild-type osmCmRNA and the corresponding amino acid sequence are shown on the left. White arrowhead marks translation start site. Red and blue arrowheads point to the drug-induced arrest sites within the coding sequences of each of the three used mRNAs. Note that due to the large size of the ribosome, the reverse transcriptase used in the toe-printing assay stops 16 nucleotides downstream of the codon located in the P-site. Because osmC mRNA template harbors other downstream alanine codons, CHL also caused ribosome stalling at these downstream sites subsequent to the appearance of Ala, Ser, or Thr residues in the penultimate position of the peptide chain (lanes 2, 4, and 6, blue

arrowhead). The results of the toe-printing assay confirmed that the presence of the MTI or MAI tripeptide sequences in the P site of the ribosome results in CHL-dependent stalling, whereas MFI tripeptide sequence is not conducive to ribosome stalling and can serve as a negative control. Experiments were repeated twice independently with similar results.



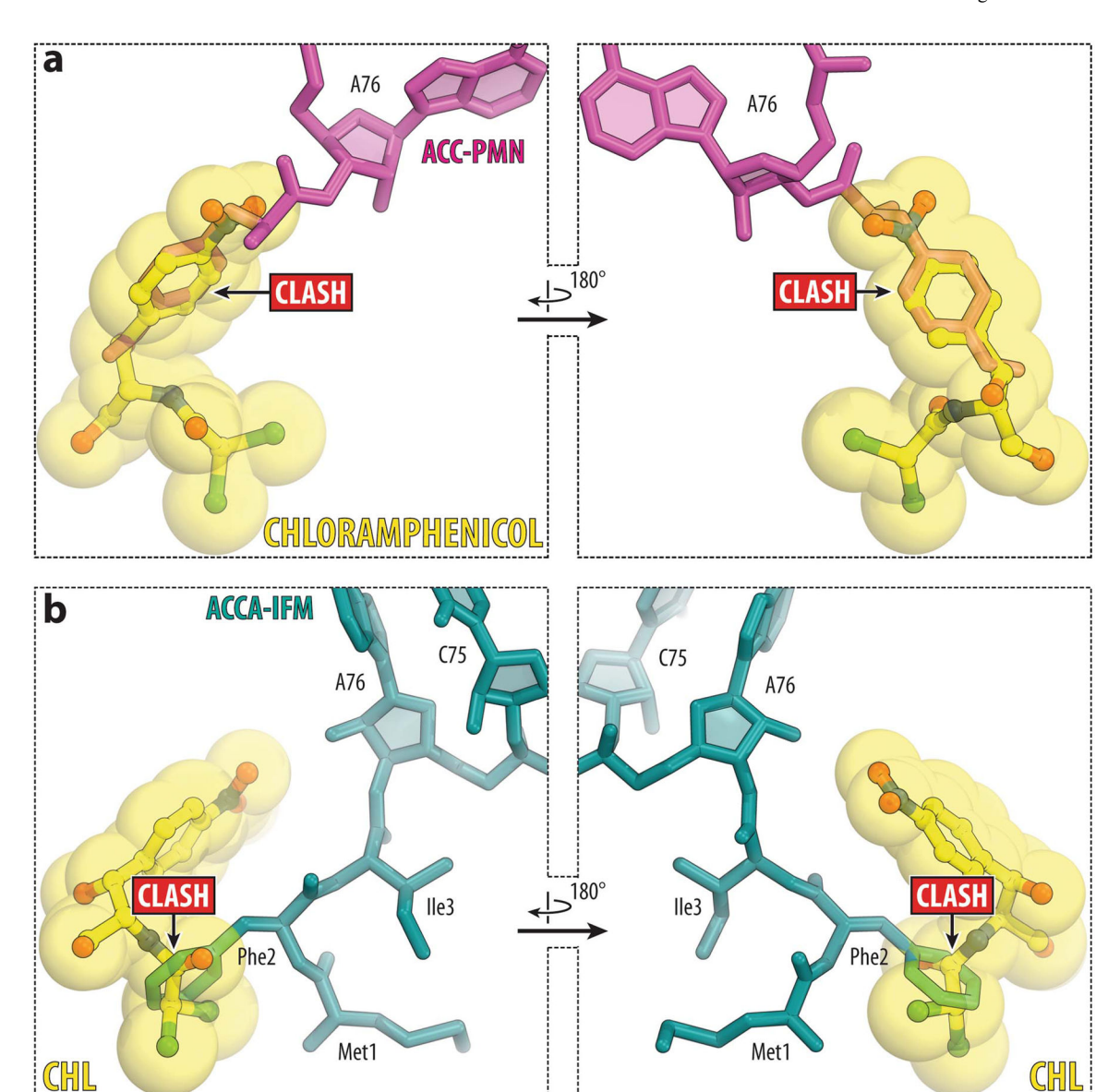
Extended Data Fig. 3. Superpositioning of the structures of short tRNA analogs with the aminoacylated full-length tRNAs.

(a, b, c) Comparisons of the 70S ribosome structures carrying ACC-Pmn (magenta) in the A site and either ACCA-ITM (a, green), or ACCA-IAM (b, blue), or ACCA-IFM (c, teal) short peptidyl tRNA analogs in the P site with the previous structure of ribosome-bound full-length aminoacyl-tRNAs (PDB entry 6ZHW<sup>24</sup>). All structures were aligned based on domain V of the 23S rRNA. (d, e, f) Comparisons of the positions of key 23S rRNA nucleotides around the PTC in the same structures. Note that there are no significant differences in the positions of A- or P-site substrates or the PTC nucleotides.



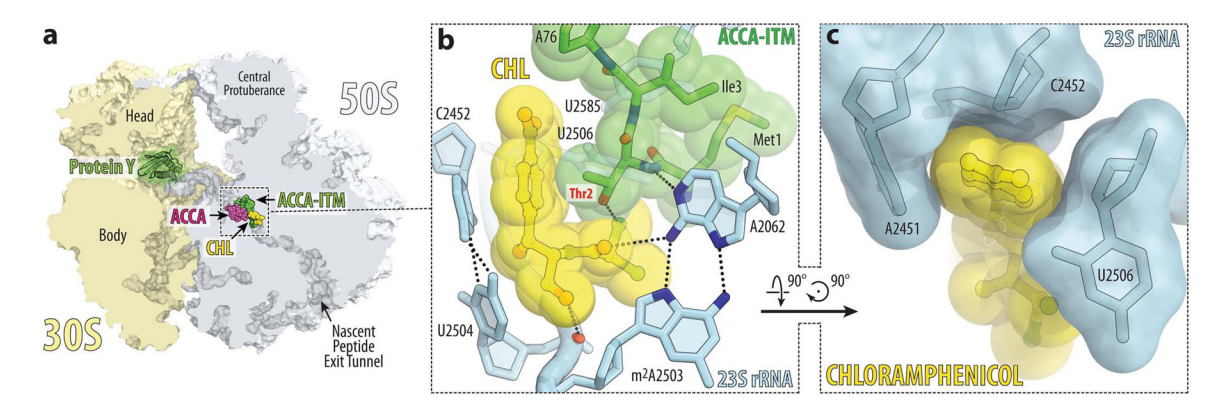
Extended Data Fig. 4. Comparison of the structure of short MTI-tripeptidyl-tRNA analog with the structures of other ribosome-bound peptidyl-tRNAs.

Superpositioning of *Thermus themophilus* 70S ribosome structure carrying A-site ACC-Pmn (magenta) and P-site ACCA-ITM tripeptidyl-tRNA analog (green) with the previously reported structures of *Escherichia coli* 70S ribosome in complex with full-length P-site peptidyl tRNA carrying SpeFL (a) or VemP (b) stalling peptides (PDB entry 6TC3<sup>26</sup> and 5NWY<sup>27</sup>, respectively). All structures were aligned based on domain V of the 23S rRNA. Note that the full-length peptidyl-tRNAs feature ester bonds between the ribose of A76 nucleotide of tRNA and the peptide moiety. Also, note that the overall path of the MTI tripeptide in our structure is similar to the trajectories of the SpeFL or VemP stalling peptides in the NPET.



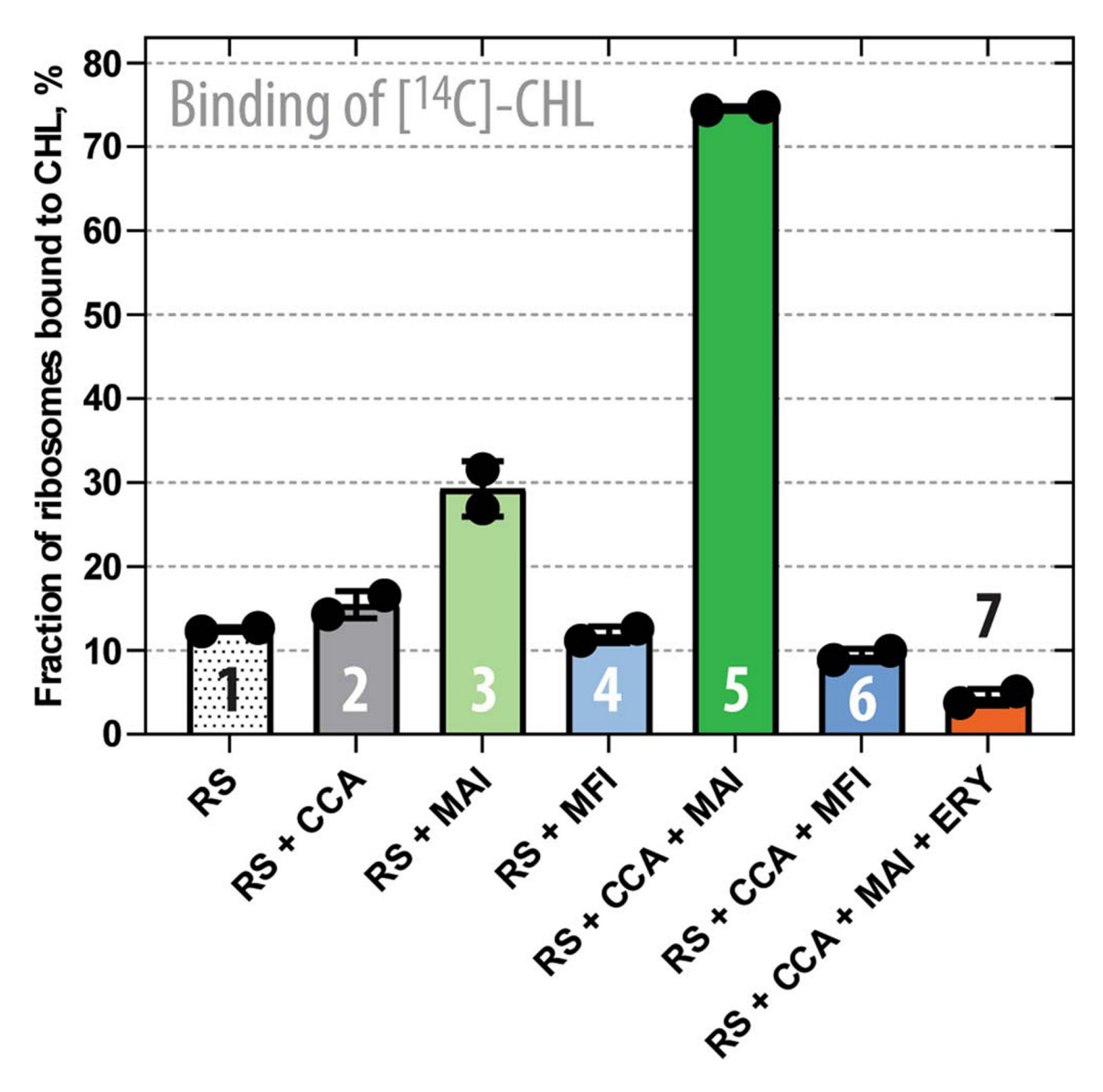
Extended Data Fig. 5. Superposition of the ribosome-bound CHL with the structures of ribosome-bound aa-tRNA and peptidyl-tRNA analogs.

(a) Superposition of CHL with the A-site-bound aa-tRNA analog ACC-Pmn. (b) Superposition of CHL with the P-site-bound peptidyl-tRNA analog ACCA-IFM. The structure of CHL is from PDB entry 6ND5<sup>10</sup>. The structures were aligned based on domain V of the 23S rRNA. Note that the side chains of the incoming amino acid in the A site (a) or the penultimate amino acid of the peptide in the P site (b) clash with CHL in its canonical binding site.



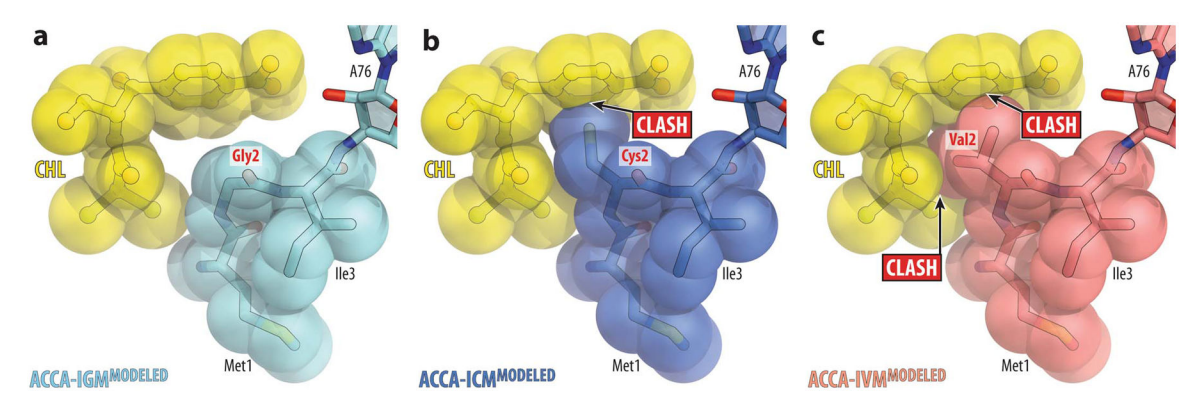
# Extended Data Fig. 6. Structure of CHL in complex with the 70S ribosome and MTI-tripeptidyl-tRNA analog.

(a) Overview of the CHL binding site (yellow) in the *Thermus thermophilus* 70S ribosome in complex with the short tripeptidyl-tRNA analogs viewed as a cross-cut section through the nascent peptide exit tunnel. The 30S subunit is shown in light yellow; the 50S subunit is in light blue; ribosome-bound protein Y is colored in green. (b, c) Close-up views of CHL bound in the PTC, highlighting H-bond interactions (dashed lines) and the intercalation of the nitrobenzyl group into the A-site cleft formed by nucleotides A2451 and C2452 of the 23S rRNA. Note that the side chain of the Thr2 residue of the MTI tripeptide directly interacts with the ribosome-bound CHL.



Extended Data Fig. 7. Short MAI and MFI tripeptidyl-tRNA analogs exhibit opposite effects on CHL binding *in vitro*.

Binding of radioactively labeled [<sup>14</sup>C]-CHL to the *Thermus thermophilus* 50S ribosomal subunits (RS) was measured using fragment reaction assay<sup>52</sup> in the presence of the indicated A- and P-site substrates. The synthetic oligonucleotide CACCA (analog of the CCA-end of deacylated tRNA) and ACCA-IAM/IFM compounds (analogs of the CCA-ends of the peptidyl-tRNAs carrying MAI or MFI tripeptide moieties) serving as the A- and P-site substrates, respectively, were the same as those used for the structural studies. Error bars represent standard deviations of the mean of two independent measurements.



Extended Data Fig. 8. In silico modeling of MGI-, MCI-, and MVI-tripeptidyl-tRNA analogs in the presence of CHL.

Using the structure of MAI-tripeptidyl-tRNA analog bound to the ribosome in the presence of CHL as a reference, the second alanine residue was mutated either to glycine (a), cysteine (b), or valine (c) and assessed the modeled structures for sterical clashes.

#### **ACKNOWLEDGMENTS**

We thank Julia Thaler (Innsbruck) for synthetic support on the RNA-peptide conjugates. We thank Dr. Alexander Mankin for his critical reading of the manuscript, as well as Dr. Kiira Ratia and Dr. Maxim Svetlov for valuable suggestions. We thank the staff at NE-CAT beamlines 24ID-C and 24ID-E for help with data collection and freezing of the crystals, especially Drs. Malcolm Capel, Frank Murphy, Igor Kourinov, Anthony Lynch, Surajit Banerjee, David Neau, Jonathan Schuermann, Narayanasami Sukumar, James Withrow, Kay Perry, Ali Kaya, and Cyndi Salbego.

This work is based upon research conducted at the Northeastern Collaborative Access Team beamlines, which are funded by the National Institute of General Medical Sciences from the National Institutes of Health [P30-GM124165 to NE-CAT]. The Eiger 16M detector on 24-ID-E beamline is funded by an NIH-ORIP HEI grant [S10-OD021527 to NE-CAT]. This research used resources of the Advanced Photon Source, a U.S. Department of Energy (DOE) Office of Science User Facility operated for the DOE Office of Science by Argonne National Laboratory under Contract No. DE-AC02-06CH11357.

This work was supported by the National Institutes of Health [R01-GM132302 to Y.S.P.], the National Science Foundation [MCB-1951405 to N.V.-L.], the Illinois State startup funds [to Y.S.P.], and Austrian Science Fund FWF [P31691 and F8011 to R.M.].

#### **DATA AVAILABILITY STATEMENT**

Coordinates and structure factors were deposited in the RCSB Protein Data Bank with accession codes:

- 7RQA for the *T. thermophilus* 70S ribosome in complex with protein Y, A-site aminoacyl-tRNA analog ACC-Pmn, and P-site peptidyl-tRNA analog ACCA-ITM:
- 7RQB for the *T. thermophilus* 70S ribosome in complex with protein Y, A-site aminoacyl-tRNA analog ACC-Pmn, and P-site peptidyl-tRNA analog ACCA-IAM;
- 7RQC for the *T. thermophilus* 70S ribosome in complex with protein Y, A-site aminoacyl-tRNA analog ACC-Pmn, and P-site peptidyl-tRNA analog ACCA-IFM;

7RQD for the *T. thermophilus* 70S ribosome in complex with protein Y, A-site deacylated tRNA analog CACCA, P-site peptidyl-tRNA analog ACCA-ITM, and chloramphenicol;

7RQE for the *T. thermophilus* 70S ribosome in complex with protein Y, A-site deacylated tRNA analog CACCA, P-site peptidyl-tRNA analog ACCA-IAM, and chloramphenicol;

All previously published structures that were used in this work for structural comparisons were retrieved from the RCSB Protein Data Bank: PDB entries 6XHW, 6WDD, 1VQN, 1VY7, 6TC3, 5NWY, 6ND5, 3CPW.

No sequence data were generated in this study.

#### REFERENCES FOR THE MAIN TEXT

- 1. Blanchard SC, Cooperman BS & Wilson DN Probing translation with small-molecule inhibitors. Chem. Biol 17, 633–645 (2010). [PubMed: 20609413]
- Barnhill AE, Brewer MT & Carlson SA Adverse effects of antimicrobials via predictable or idiosyncratic inhibition of host mitochondrial components. Antimicrob. Agents Chemother 56, 4046–4051 (2012). [PubMed: 22615289]
- Jones CN, Miller C, Tenenbaum A, Spremulli LL & Saada A Antibiotic effects on mitochondrial translation and in patients with mitochondrial translational defects. Mitochondrion 9, 429–437 (2009). [PubMed: 19671450]
- 4. Singh R, Sripada L & Singh R Side effects of antibiotics during bacterial infection: mitochondria, the main target in host cell. Mitochondrion 16, 50–54 (2014). [PubMed: 24246912]
- Li CH, Cheng YW, Liao PL, Yang YT & Kang JJ Chloramphenicol causes mitochondrial stress, decreases ATP biosynthesis, induces matrix metalloproteinase-13 expression, and solid-tumor cell invasion. Toxicol. Sci 116, 140–150 (2010). [PubMed: 20338993]
- Cohen BH & Saneto RP Mitochondrial translational inhibitors in the pharmacopeia. Biochim. Biophys. Acta 1819, 1067–1074 (2012). [PubMed: 22421540]
- 7. Syriopoulou VP, Harding AL, Goldmann DA & Smith AL In vitro antibacterial activity of fluorinated analogs of chloramphenicol and thiamphenicol. Antimicrob. Agents Chemother 19, 294–297 (1981). [PubMed: 6957162]
- 8. Dunkle JA, Xiong L, Mankin AS & Cate JH Structures of the Escherichia coli ribosome with antibiotics bound near the peptidyl transferase center explain spectra of drug action. Proc. Natl. Acad. Sci. USA 107, 17152–17157 (2010). [PubMed: 20876128]
- 9. Bulkley D, Innis CA, Blaha G & Steitz TA Revisiting the structures of several antibiotics bound to the bacterial ribosome. Proc. Natl. Acad. Sci. USA 107, 17158–17163 (2010). [PubMed: 20876130]
- Svetlov MS et al. High-resolution crystal structures of ribosome-bound chloramphenicol and erythromycin provide the ultimate basis for their competition. RNA 25, 600–606 (2019). [PubMed: 30733327]
- 11. Drainas D, Kalpaxis DL & Coutsogeorgopoulos C Inhibition of ribosomal peptidyltransferase by chloramphenicol. Kinetic studies. Eur. J. Biochem 164, 53–58 (1987). [PubMed: 3549307]
- 12. Kucan Z & Lipmann F Differences in chloramphenicol sensitivity of cell-free amino acid polymerization systems. J. Biol. Chem 239, 516–520 (1964). [PubMed: 14169152]
- 13. Vazquez D Antibiotics affecting chloramphenicol uptake by bacteria. Their effect on amino acid incorporation in a cell-free system. Biochim. Biophys. Acta 114, 289–295 (1966). [PubMed: 5329271]
- 14. Cannon M The puromycin reaction and its inhibition by chloramphenicol. Eur. J. Biochem 7, 137–145 (1968). [PubMed: 4884583]

15. Rheinberger HJ & Nierhaus KH Partial release of AcPhe-Phe-tRNA from ribosomes during poly(U)-dependent poly(Phe) synthesis and the effects of chloramphenicol. Eur. J. Biochem 193, 643–650 (1990). [PubMed: 2249685]

- 16. Lovett PS Translation attenuation regulation of chloramphenicol resistance in bacteria -a review. Gene 179, 157–162 (1996). [PubMed: 8955642]
- 17. Lovett PS Translational attenuation as the regulator of inducible cat genes. J. Bacteriol 172, 1–6 (1990). [PubMed: 2403536]
- 18. Marks J et al. Context-specific inhibition of translation by ribosomal antibiotics targeting the peptidyl transferase center. Proc. Natl. Acad. Sci. USA 113, 12150–12155 (2016). [PubMed: 27791002]
- 19. Choi J et al. Dynamics of the context-specific translation arrest by chloramphenicol and linezolid. Nat. Chem. Biol 16, 310–317 (2020). [PubMed: 31844301]
- 20. Orelle C et al. Tools for characterizing bacterial protein synthesis inhibitors. Antimicrob. Agents Chemother 57, 5994–6004 (2013). [PubMed: 24041905]
- 21. Moroder H et al. Non-hydrolyzable RNA-peptide conjugates: a powerful advance in the synthesis of mimics for 3'-peptidyl tRNA termini. Angew. Chem. Int. Ed. Engl 48, 4056–4060 (2009). [PubMed: 19396850]
- 22. Hartz D, McPheeters DS, Traut R & Gold L Extension inhibition analysis of translation initiation complexes. Methods Enzymol. 164, 419–425 (1988). [PubMed: 2468068]
- Polikanov YS, Steitz TA & Innis CA A proton wire to couple aminoacyl-tRNA accommodation and peptide-bond formation on the ribosome. Nat. Struct. Mol. Biol 21, 787–793 (2014). [PubMed: 25132179]
- 24. Svetlov MS et al. Structure of Erm-modified 70S ribosome reveals the mechanism of macrolide resistance. Nat. Chem. Biol 17, 412–420 (2021). [PubMed: 33462493]
- 25. Loveland AB, Demo G & Korostelev AA Cryo-EM of elongating ribosome with EF-Tu\*GTP elucidates tRNA proofreading. Nature 584, 640–645 (2020). [PubMed: 32612237]
- 26. Herrero Del Valle A et al. Ornithine capture by a translating ribosome controls bacterial polyamine synthesis. Nat. Microbiol 5, 554–561 (2020). [PubMed: 32094585]
- 27. Su T et al. The force-sensing peptide VemP employs extreme compaction and secondary structure formation to induce ribosomal stalling. Elife 6(2017).
- 28. Goto Y & Suga H Translation initiation with initiator tRNA charged with exotic peptides. J. Am. Chem. Soc 131, 5040–5041 (2009). [PubMed: 19301866]
- 29. Tereshchenkov AG et al. Binding and action of amino acid analogs of chloramphenicol upon the bacterial ribosome. J. Mol. Biol 430, 842–852 (2018). [PubMed: 29410130]
- 30. Chen CW et al. Binding and action of triphenylphosphonium analog of chloramphenicol upon the bacterial ribosome. Antibiotics (Basel) 10(2021).
- 31. Nishio M The CH/pi hydrogen bond in chemistry. Conformation, supramolecules, optical resolution and interactions involving carbohydrates. Phys. Chem. Chem. Phys 13, 13873–13900 (2011). [PubMed: 21611676]
- 32. Fersht AR The hydrogen bond in molecular recognition. Trends in Biochemical Sciences 12, 301–304 (1987).
- 33. Becker AH, Oh E, Weissman JS, Kramer G & Bukau B Selective ribosome profiling as a tool for studying the interaction of chaperones and targeting factors with nascent polypeptide chains and ribosomes. Nat. Protoc 8, 2212–2239 (2013). [PubMed: 24136347]
- 34. Mohammad F, Woolstenhulme CJ, Green R & Buskirk AR Clarifying the translational pausing landscape in bacteria by ribosome profiling. Cell Rep. 14, 686–694 (2016). [PubMed: 26776510]
- 35. Ippolito JA et al. Crystal structure of the oxazolidinone antibiotic linezolid bound to the 50S ribosomal subunit. J. Med. Chem 51, 3353–3356 (2008). [PubMed: 18494460]
- 36. Tsai K et al. Structural basis for context-specific inhibition of translation by oxazolidinone antibiotics. Nat. Struct. Mol. Biol (2021).
- 37. Vazquez-Laslop N & Mankin AS Context-specific action of ribosomal antibiotics. Annu. Rev. Microbiol 72, 185–207 (2018). [PubMed: 29906204]

38. Vazquez-Laslop N & Mankin AS How macrolide antibiotics work. Trends Biochem. Sci 43, 668–684 (2018). [PubMed: 30054232]

- 39. Arenz S et al. Drug sensing by the ribosome induces translational arrest via active site perturbation. Mol. Cell 56, 446–452 (2014). [PubMed: 25306253]
- 40. Arenz S et al. A combined cryo-EM and molecular dynamics approach reveals the mechanism of ErmBL-mediated translation arrest. Nat. Commun 7, 12026 (2016). [PubMed: 27380950]
- 41. Beckert B et al. Structural and mechanistic basis for translation inhibition by macrolide and ketolide antibiotics. Nat. Commun 12, 4466 (2021). [PubMed: 34294725]
- 42. Hedstrom L IMP dehydrogenase: structure, mechanism, and inhibition. Chem. Rev 109, 2903–2928 (2009). [PubMed: 19480389]
- 43. Steger J et al. Efficient access to nonhydrolyzable initiator tRNA based on the synthesis of 3'-azido-3'-deoxyadenosine RNA. Angew. Chem. Int. Ed. Engl 49, 7470–7472 (2010). [PubMed: 21038451]
- 44. Steger J & Micura R Functionalized polystyrene supports for solid-phase synthesis of glycyl-, alanyl-, and isoleucyl-RNA conjugates as hydrolysis-resistant mimics of peptidyl-tRNAs. Bioorg. Med. Chem 19, 5167–5174 (2011). [PubMed: 21807524]
- Geiermann AS, Polacek N & Micura R Native chemical ligation of hydrolysis-resistant 3'peptidyl-tRNA mimics. J. Am. Chem. Soc 133, 19068–19071 (2011). [PubMed: 22050598]
- 46. Melnikov SV et al. Mechanistic insights into the slow peptide bond formation with D-amino acids in the ribosomal active site. Nucleic Acids Res. 47, 2089–2100 (2019). [PubMed: 30520988]
- 47. Polikanov YS, Blaha GM & Steitz TA How hibernation factors RMF, HPF, and YfiA turn off protein synthesis. Science 336, 915–918 (2012). [PubMed: 22605777]
- 48. Polikanov YS, Melnikov SV, Soll D & Steitz TA Structural insights into the role of rRNA modifications in protein synthesis and ribosome assembly. Nat. Struct. Mol. Biol 22, 342–344 (2015). [PubMed: 25775268]
- 49. Almutairi MM et al. Co-produced natural ketolides methymycin and pikromycin inhibit bacterial growth by preventing synthesis of a limited number of proteins Nucleic Acids Res. 45, 9573–9582 (2017). [PubMed: 28934499]
- 50. Mitcheltree MJ et al. A synthetic antibiotic class overcoming bacterial multidrug resistance. Nature 599, 507–512 (2021). [PubMed: 34707295]
- Wilson DN et al. The oxazolidinone antibiotics perturb the ribosomal peptidyl-transferase center and effect tRNA positioning. Proc. Natl. Acad. Sci. USA 105, 13339–13344 (2008). [PubMed: 18757750]
- 52. Monro RE Ribosomal peptidyltransferase: The fragment reaction. Methods Enzymol. 20, 472–481 (1971).

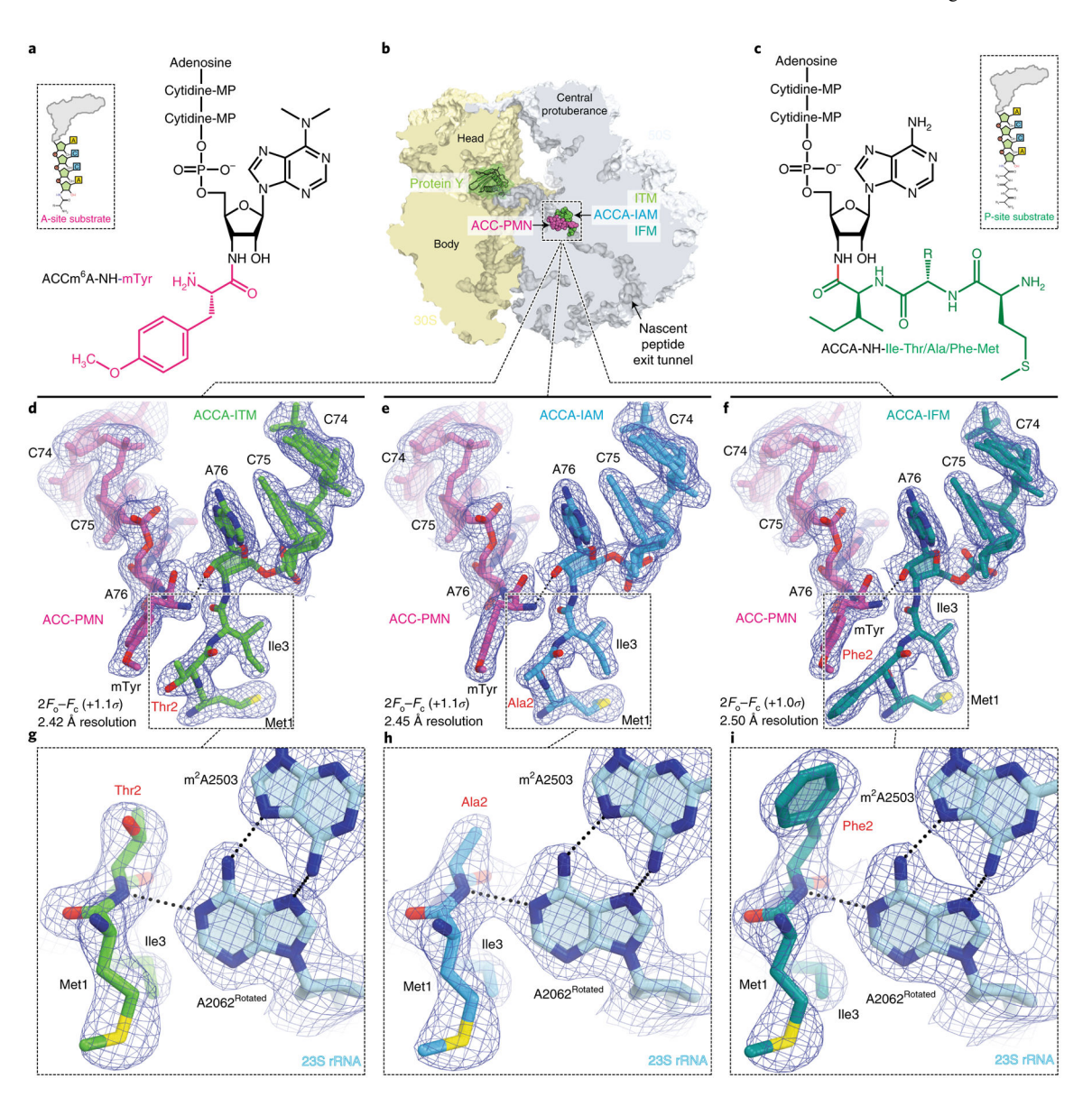


Figure 1  $\mid$ . Electron density maps of the short tripeptidyl-tRNA analogs bound to the *T. thermophilus* 70S ribosome in the absence of CHL.

(a, c) Chemical structures of the hydrolysis-resistant aminoacyl-tRNA mimic ACC-Puromycin (a), and the peptidyl-tRNA mimics ACCA-ITM, ACCA-IAM, or ACCA-IFM (c). The amino acid moiety of ACC-Puromycin and peptide moiety of tripeptidyl-tRNA analogs are highlighted in purple and green, respectively. (b) Overview of the T. thermophilus 70S ribosome structures featuring short tRNA analogs viewed as a cross-cut section through the nascent peptide exit tunnel. The 30S subunit is shown in light yellow; the 50S subunit is in light blue; ribosome-bound protein Y is colored in green. (d-f)  $2F_o$ - $F_c$  electron difference Fourier maps of ACC-PMN (purple) and either MTI-tripeptidyl-tRNA (d, green), or MAI-tripeptidyl-tRNA (e, blue), or MFI-tripeptidyl-tRNA (f, teal) analogs. The refined models of short tRNA analogs are displayed in their respective electron density maps after the refinement (blue mesh). The overall resolution of the corresponding structures and the contour levels of the depicted electron density maps are shown in the bottom left

corner of each panel. (g-i) Close-up views of the MTI (g), MAI (h) or MFI (i) tripeptides interacting with the nucleotides of the 23S rRNA (light blue). Note that regardless of the nature of amino acid in the  $2^{nd}$  position, all tripeptides have nearly identical paths in the ribosome exit tunnel.

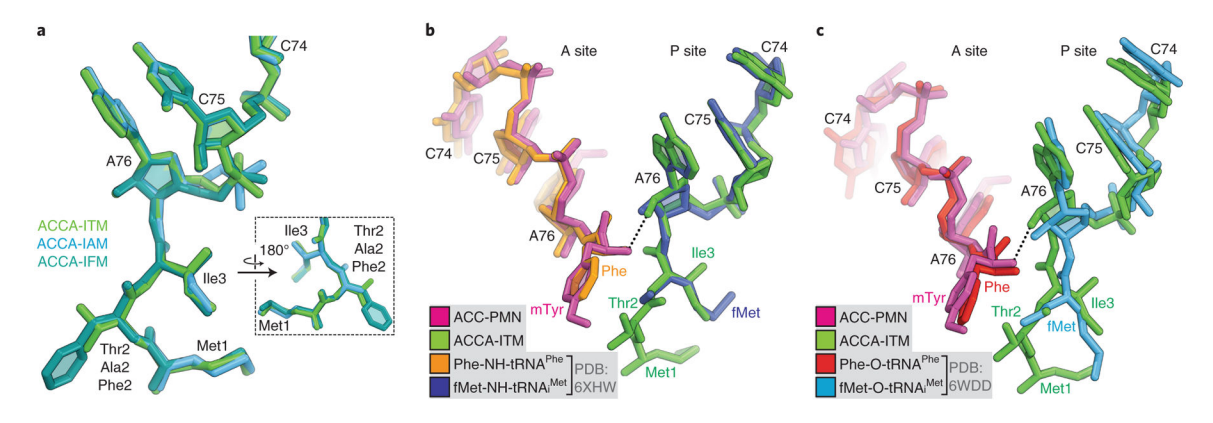


Figure 2  $\mid$ . Comparison of the structures of short tripeptidyl-tRNA analogs reveals no significant differences between each other and with full-length tRNAs.

(a) Superpositioning of the current 70S ribosome structures in complex with short tripeptidyl-tRNA analogs carrying MTI (green), MAI (blue), and MFI (teal) tripeptide sequences with each other. Note that the path of the growing polypeptide chain in the exit tunnel is not affected by the nature of the amino acid in the -1 position. (b, c) Comparison of our 70S ribosome structure carrying ACCA-PMN (magenta) and ACCA-ITM (green) short tRNA analogs in the A and P sites, respectively, with the previously reported structures of ribosome-bound full-length aminoacyl-tRNAs featuring either non-hydrolyzable amide linkages (b, PDB entry 6XHW<sup>24</sup>) or native ester bonds (c, PDB entry 6WDD<sup>25</sup>) between the amino acid moiety and the ribose of A76 nucleotides. All structures were aligned based on domain V of the 23S rRNA. Note that, because the differences between the compared structures of the A- and P-site substrates are within experimental error, the short tRNA mimics represent functionally meaningful analogs of full-length tRNAs. Also, note that the amino acid moieties both in the A and P sites have very similar orientations regardless of whether or not the linkages are native or non-hydrolyzable.

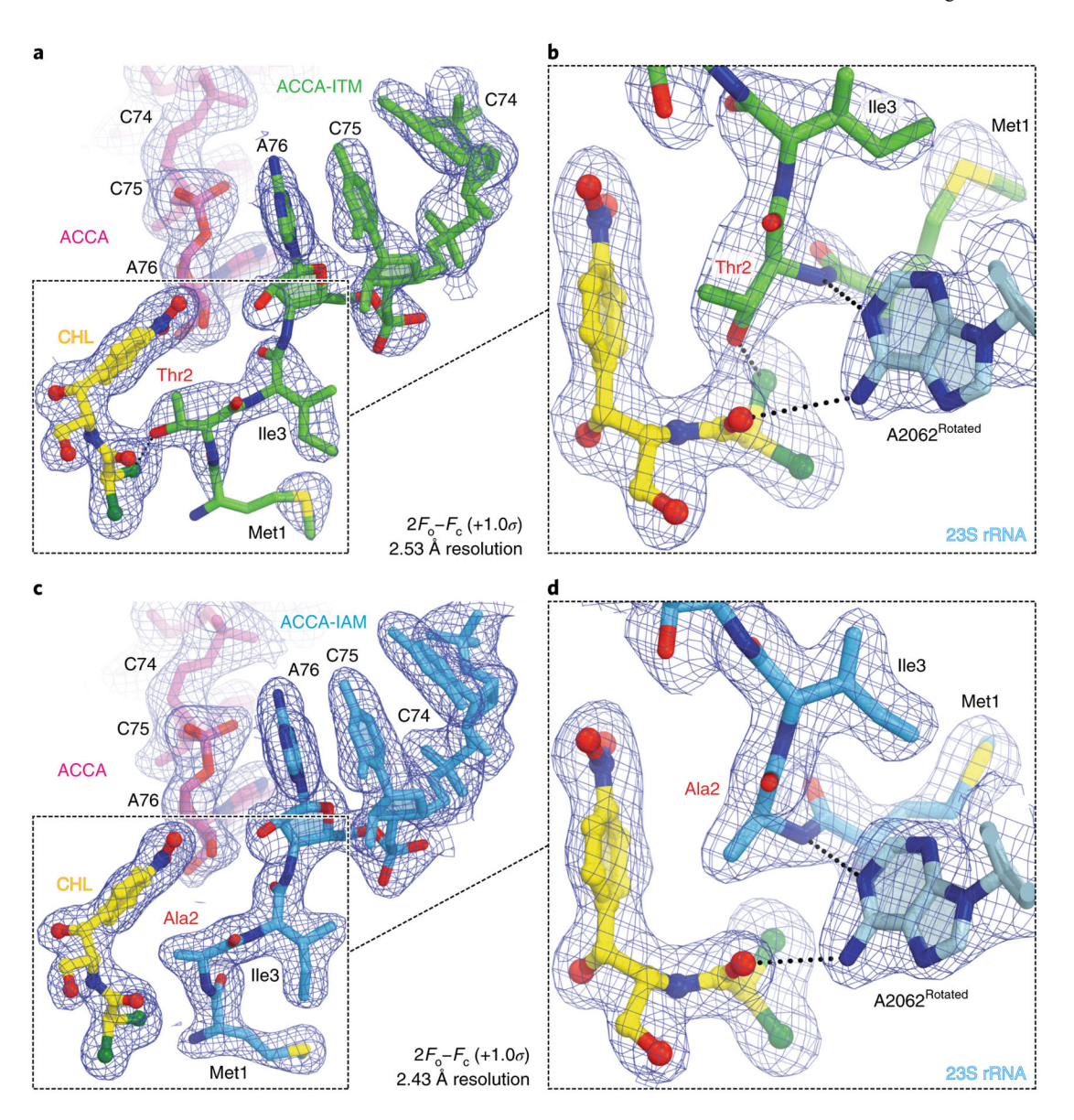


Figure 3 |. Electron density maps of the short tripeptidyl-tRNA analogs bound to the T. thermophilus 70S ribosome in the presence of CHL.  $2F_o$ - $F_c$  electron density maps of the A-site ACCA (purple) and P-site short MTI-tripeptidyl-tRNA ( $\mathbf{a}$ ,  $\mathbf{b}$ ; green) or MAI-tripeptidyl-tRNA ( $\mathbf{c}$ ,  $\mathbf{d}$ ; blue) analogs bound to the T.

thermophilus 70S ribosome in the presence of CHL (yellow).

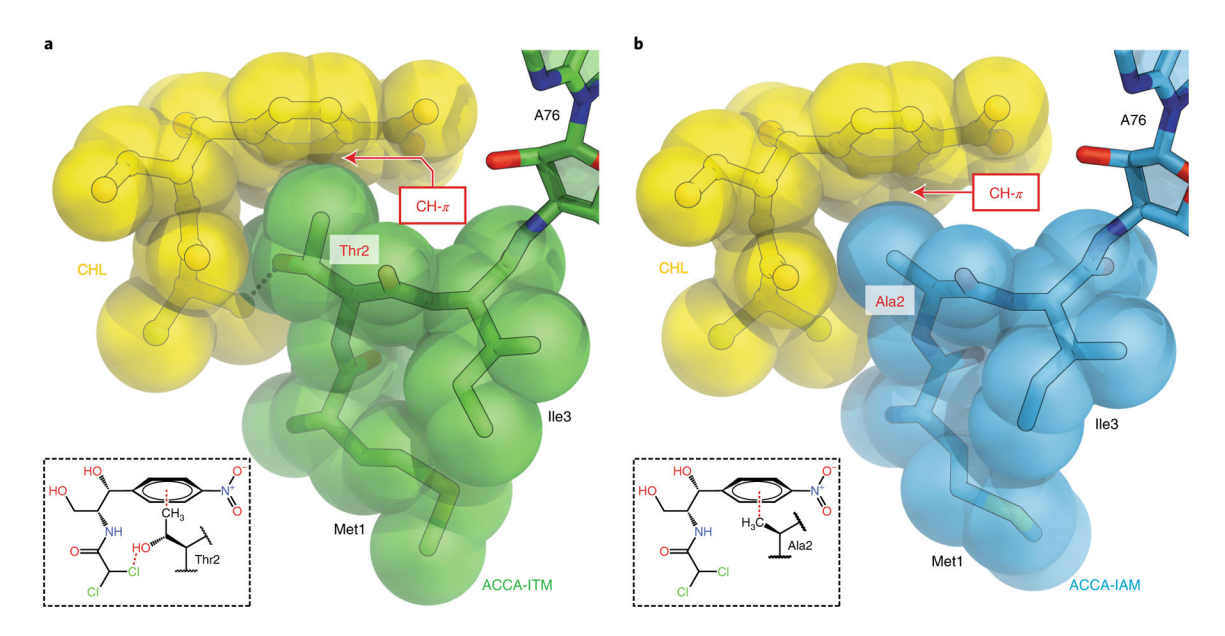


Figure 4  $\mid$ . CHL directly interacts with the stalling peptides MTI and MAI in the *T. thermophilus* 70S ribosome.

Close-up views of the MTI (a) or MAI (b) tripeptides interacting with the CHL on the ribosome. Note that the side chains of penultimate threonine or alanine residues of the nascent peptide form H-bond or CH- $\pi$  interactions with the dichloroacetic and/or nitrobenzyl moieties of CHL.

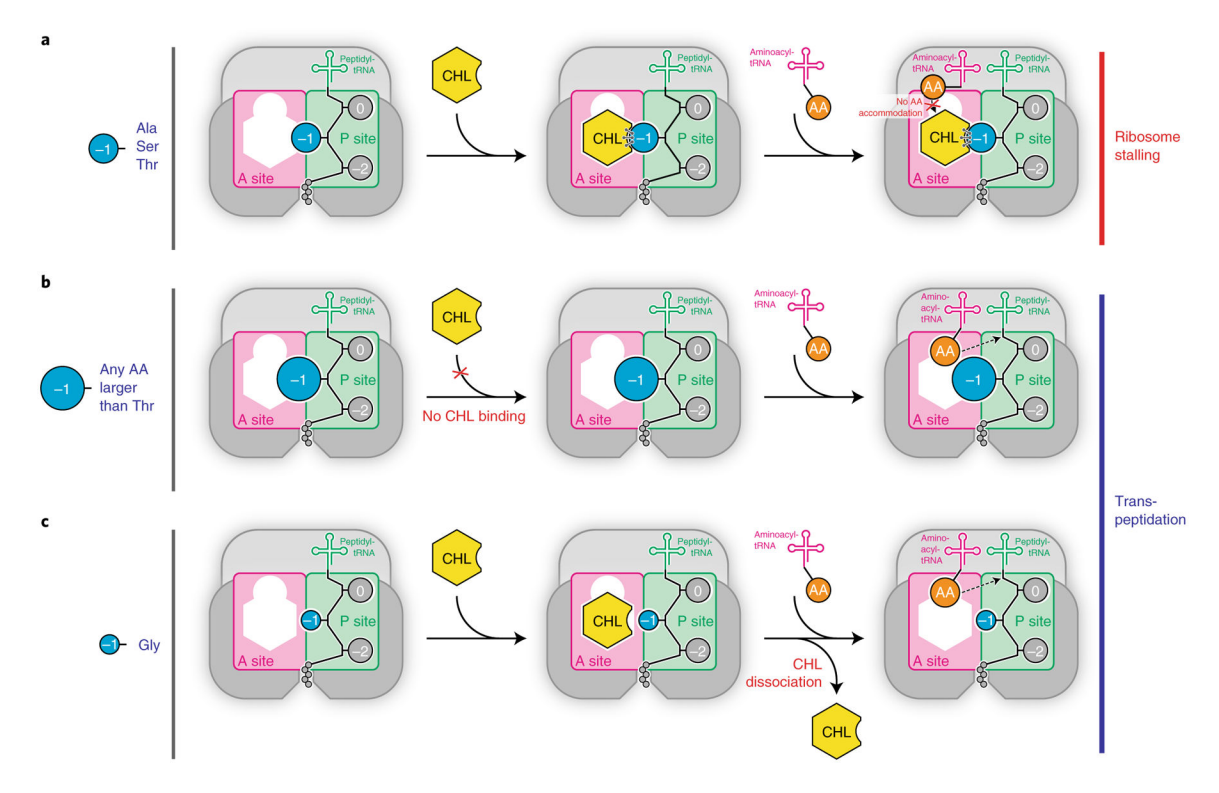


Figure 5 |. Schematic diagram illustrating the increased affinity model.

(a) When the growing polypeptide chain carries alanine, serine, or threonine (blue circle) in the penultimate position, the affinity of CHL (yellow hexagon) for the ribosome increases due to direct interactions with the side chains of these amino acids preventing accommodation of the aminoacyl moiety of the aa-tRNA into the A site and, thereby, inhibiting peptidyl transferase reaction, which results in ribosome stalling. (b) Amino acid residues with larger side chains in the penultimate position of the growing peptide are sterically incompatible with CHL preventing its binding to the ribosome. In the absence of ribosome-bound CHL, aa-tRNA normally accommodates into the ribosomal A site resulting in an unperturbed transpeptidation reaction. (c) Glycine residue in the penultimate position of the growing peptide does not interfere with the binding of CHL but also does not increase the drug's affinity for the ribosome. As a result, loosely bound CHL is displaced from the ribosomal A site by the incoming aa-tRNA, which, after accommodation, can normally react with the P-site substrate. Small and large ribosomal subunits are highlighted in shades of grey. A and P sites are highlighted in magenta and green, respectively. Amino acids of the growing polypeptide chain are shown by grey circles with the penultimate amino acid residue highlighted in blue.

Syroegin et al. Page 32

Table 1 |

X-ray data collection and refinement statistics.

	70S-PY complex with ACCA-ITM and ACC-Pmn PDB entry 7RQA	70S-PY complex with ACCA-IAM and ACC-Pmn PDB entry 7RQB	70S-PY complex with ACCA-IFM and ACC-Pmn PDB entry 7RQC	70S-PY complex with ACCA-ITM, ACCA, and CHL PDB entry 7RQD	70S-PY complex with ACCA-IAM, ACCA, and CHL PDB entry 7RQE
Data collection					
Space group	P2 <sub>1</sub> 2 <sub>1</sub> 2 <sub>1</sub>	$P2_12_12_1$	$P2_12_12_1$	P2 <sub>1</sub> 2 <sub>1</sub> 2 <sub>1</sub>	$P2_{1}2_{1}2_{1}$
Cell dimensions					
a, b, c (Å)	209.64, 448.67, 619.79	209.61, 448.45, 618.45	209.32, 449.63, 620.21	209.71, 449.95, 621.20	209.81, 449.56, 621.47
$\alpha,\beta,\gamma(^\circ)$	90.0, 90.0, 90.0	90.0, 90.0, 90.0	90.0, 90.0, 90.0	90.0, 90.0, 90.0	90.0, 90.0, 90.0
Resolution (Å)	224–2.42 (2.48– 2.42) <sup>a</sup>	309–2.45 (2.51– 2.45) <sup>a</sup>	310–2.50 (2.56– 2.50) <sup>b</sup>	310–2.53 (2.60– 2.53) <sup>a</sup>	311–2.43 (2.49– 2.43) <sup>b</sup>
R merge	18.1 (139.7)	20.7 (208.0)	24.8 (240.9)	15.7 (134.5)	24.0 (211.9)
$I/\sigma I$	7.18 (1.0) <sup>c</sup>	6.75 (1.00) <sup>d</sup>	9.53 (1.07) <sup>e</sup>	$8.65 (1.00)^f$	8.20 (1.00) <sup>g</sup>
Completeness (%)	99.8 (99.8)	99.9 (100.0)	99.9 (99.7)	98.8 (96.3)	99.8 (99.7)
Redundancy	5.64 (5.22)	6.99 (7.20)	12.06 (11.89)	4.65 (4.06)	9.30 (9.44)
Refinement					
Resolution (Å)	2.40	2.45	2.50	2.50	2.40
No. reflections	2,234,711	2,100,392	1,985,988	1,965,432	2,248,412
$R_{ m work}$ / $R_{ m free}$	23.9/28.9	20.6/24.5	23.0/27.9	22.9/28.0	22.6/27.0
No. atoms					
Protein	93,149	93,145	93,157	93,149	93,145
Ligand/ion	195,168	195,125	195,155	195,113	195,120
Water	8,599	8,013	8,298	8,261	8,499
B factors					
Protein	56.7	60.8	58.6	56.7	57.9
Ligand/ion	54.2	57.0	55.5	53.9	54.5
Water	40.1	43.6	39.9	39.1	41.0
r.m.s. deviations					
Bond lengths (Å)	0.005	0.004	0.004	0.005	0.004
Bond angles (°)	0.913	0.878	0.871	0.878	0.873

Values in parentheses are for the highest-resolution shell.

<sup>&</sup>lt;sup>a</sup>Diffraction data from a **single crystal** were used to obtain the structure.

 $b_{\mbox{Diffraction data from }\mbox{two }\mbox{crystals}}$  were used to obtain the structure.

 $<sup>^{</sup>C}$ I/ $\sigma$ I = 2 at 2.68Å resolution.

 $d_{I/\sigma I} = 2$  at 2.70Å resolution.

 $e_{\text{I/}\sigma\text{I}} = 2 \text{ at } 2.72\text{Å resolution.}$ 

 $f_{\rm I/\sigma I} = 2$  at 2.80Å resolution.

 $g_{\text{I}/\sigma\text{I}} = 2$  at 2.69Å resolution.